MASTER COPY KEEP THIS COPY FOR REPRODUCTION PURPOSES

AD-A260 592

TION PAGE

Form Approved
OMB No 0704-0188

1.	Sept. 30, 1992	3. REPORT TYPE AND DATES COVERED: Final Report 8/89 - 8/92

4. TITLE AND SUBTITLE
Second-Harmonic Generation in Optical Fibers and Glass
Final Report

5. FUNDING NUMBERS
DAAL03-89-[illegible]-0077

6. AUTHOR(S)
Vincent G. Dominic

DTIC ELECTE FEB 1 [illegible]

7. PERFORMING ORGANIZATION NAME(S) AND ADDRESS(ES)
Electrical Engineering Dept.
University of Southern California
Los Angeles, CA 90089-0484

8. PERFORMING ORGANIZATION REPORT NUMBER

9. SPONSORING/MONITORING AGENCY NAME(S) AND ADDRESS(ES)
U. S. Army Research Office
P. O. Box 12211
Research Triangle Park, NC 27709-2211

10. SPONSORING/MONITORING AGENCY REPORT NUMBER
ARO 27005.2-EL-F

11. SUPPLEMENTARY NOTES
The view, opinions and/or findings contained in this report are those of the author(s) and should not be construed as an official Department of the Army position, policy, or decision, unless so designated by other documentation.

12a. DISTRIBUTION/AVAILABILITY STATEMENT
Approved for public release; distribution unlimited.

12b. DISTRIBUTION CODE

13. ABSTRACT (Maximum 200 words)

This is the final report for the JSEP fellowship awarded to Vincent G. Dominic. We report on our investigation into the unusual and unexpected effect of second-harmonic generation in optical fibers and optical fiber preforms. We make three important conclusions: 1) Experimental investigations into this effect are simpler and more controllable if carried out in bulk glass samples (optical fiber preforms) rather than in the optical fibers themselves. 2) The induced second-order nonlinearity arises from a DC electric field which is induced inside the glass by light beams containing a fundamental frequency (ω) and its second harmonic (2ω). 3) The light beams induce the DC electric field through a multiple-photon process. Specifically, we believe that the interference between several multi-photon ionization channels gives rise to anisotropic emission of photoelectrons. The ejected electrons create a photogalvanic current that builds the DC electric field.

14. SUBJECT TERMS
Second-Harmonic Generation, Nonlinear Optics, Optical Fibers

15. NUMBER OF PAGES
33

16. PRICE CODE

17. SECURITY CLASSIFICATION OF REPORT	18. SECURITY CLASSIFICATION OF THIS PAGE	19. SECURITY CLASSIFICATION OF ABSTRACT	20. LIMITATION OF ABSTRACT
UNCLASSIFIED	UNCLASSIFIED	UNCLASSIFIED	UL

NSN 7540-01-280-5500

Standard Form 298 (Rev 2-89)
Prescribed by ANSI Std Z39-18
298-102

93-03378 34pp

DISCLAIMER NOTICE

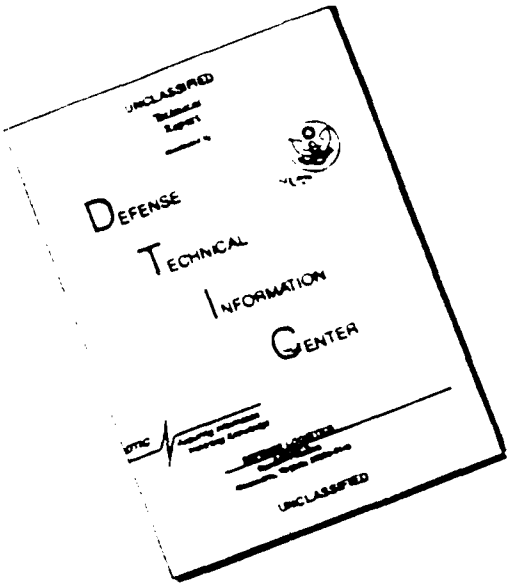

THIS DOCUMENT IS BEST QUALITY AVAILABLE. THE COPY FURNISHED TO DTIC CONTAINED A SIGNIFICANT NUMBER OF PAGES WHICH DO NOT REPRODUCE LEGIBLY.

Second-Harmonic Generation in Optical Fibers and Glass

Final Report

Vincent G. Dominic
University of Southern California
Departments of Electrical Engineering and Physics
Los Angeles, California 90089-0484

September 30, 1992

U.S. Army Research Office
ARO Proposal Number: 27005-EL-F
Grant Number: DAAL03-89-G-0077
Joint Services Electronics Program Fellowship

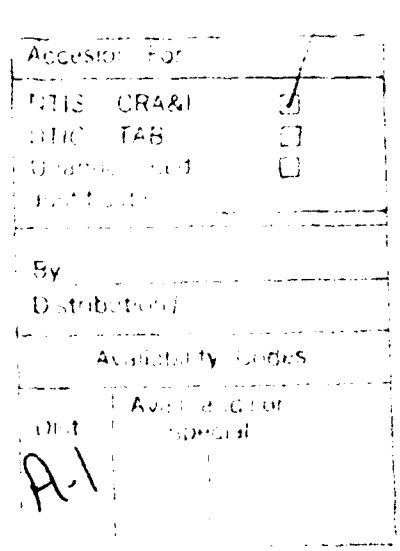

Table of Contents

Figures and Appendixes

1) FOREWORD

This final report covers the work performed by Vincent G. Dominic over the period of August 1989 to August 1992 under the auspices of the Joint Services Electronics Program (JSEP) graduate fellowship. During this fellowship, we investigated two distinct problems. First, we studied short-pulse interactions in photorefractive crystals and the use of a photorefractive crystal to measure the coherence length of laser pulses. This work has been published in two separate articles[1,2] and reprints are included in Appendix B of this report. Second, we studied second-harmonic generation in optical fibers and glass optical fiber preforms. This topic will be the main emphasis of this final report.

2) INTRODUCTION

During my JSEP fellowship tenure we studied two completely separate problems. The first problem was how short laser pulses interact inside a photorefractive crystal, such as barium titanate ($BaTiO_3$), and in particular the use of photorefractive crystals to shape the temporal profile of short pulses of light. We also developed a nice technique to determine the coherence length of mode-locked laser pulses in real time. Our coherence-length measurement technique works well for pulses having coherence times ranging from 100 ps down to about 1 ps, as discussed in Ref. 1. We also proposed a theoretical model to describe short pulse interactions inside photorefractive crystals.[2] Although I have not been directly involved in the continuation of this work, recent experiments have born out the validity of our theory.[3]

The second and primary research work sponsored by this JSEP fellowship is to understand second-harmonic generation in glass. This effect was first observed in optical fibers[4] but also appears in bulk glass samples.[5-7] This effect is interesting because, at first glance, it appears to be impossible. Glass is centrosymmetric, and thus second-order nonlinear effects are forbidden in the dipole approximation.[8] However, in 1986 Österberg and Margulis[4] observed that if they launched intense 1.064 μm laser pulses from a Q-switched Nd:YAG laser into an optical fiber, there was a slow buildup of green 532 nm light produced by the fiber. The buildup time was several hours. Stolen and Tom[9] later showed that if some externally generated 532 nm light is

launched into the fiber along with the fundamental light, then the buildup time is reduced from hours to minutes.

What happens inside the glass to remove the centrosymmetry of the material? It is now agreed that a DC electric field is induced inside the glass.[10-12] This field produces a second-order nonlinearity via the third-order susceptibility by electric field induced second-harmonic generation (EFISH). Thus the induced nonlinearity can be written:

$$\vec{\vec{\chi}}^{(2)}(-2\omega;\omega,\omega) = 3\,\vec{\vec{\chi}}^{(3)}(-2\omega;\omega,\omega,0)\cdot\vec{E}_{dc} \qquad (1)$$

where $\chi^{(3)}$ is the known third-order susceptibility tensor of glass, $\vec{E}_{dc}$ is the induced DC electric field, and $\chi^{(2)}$ is the resulting second-order nonlinearity. Here we follow the notation of Butcher and Cotter.[13] The polarization properties of the induced nonlinearity have been shown to follow the prediction of Eq. (1) in optical fibers[10] and in bulk glass samples,[12] although the spatial patterns of light generated according to Eq. (1) can be more easily seen in bulk glasses than in fibers, and this has been one of the main thrusts of our research. We have found[12] that Eq. (1) is fully born out, and that it is possible to use its polarization properties to map out the spatial profile of the induced electric field. In all of our work we have found it safe to assume that $\chi^{(3)}$ in Eq. (1) obeys Kleinman symmetry, as was also found to be true in Ref. 10.

What happens inside the glass to cause the formation of this DC electric field? Although this question has not been fully answered, and is the subject of ongoing debate, a majority of researchers now believe that the interference of two or more multi-photon ionization channels gives rise to a spatially anisotropic photoelectron current.[14-16] This photogalvanic current continues until the DC electric field it produces becomes large enough to inhibit any further separation of electrical charges. Figure 1 shows two different models which lead to this photogalvanic current. Model A shows the interference of one-photon and two-photon excitation of an electron, and the anisotropy in the direction of the ejected electron has been convincingly demonstrated in gases.[17,18] Model B is believed to be more likely in our glass samples, in which there is significant absorption at the energy equal to four infrared (1.064 μm) photons. This absorption band in glass is associated with its germanium dopant, and germanium doping is necessary to observe second-harmonic generation in fused silica. Because

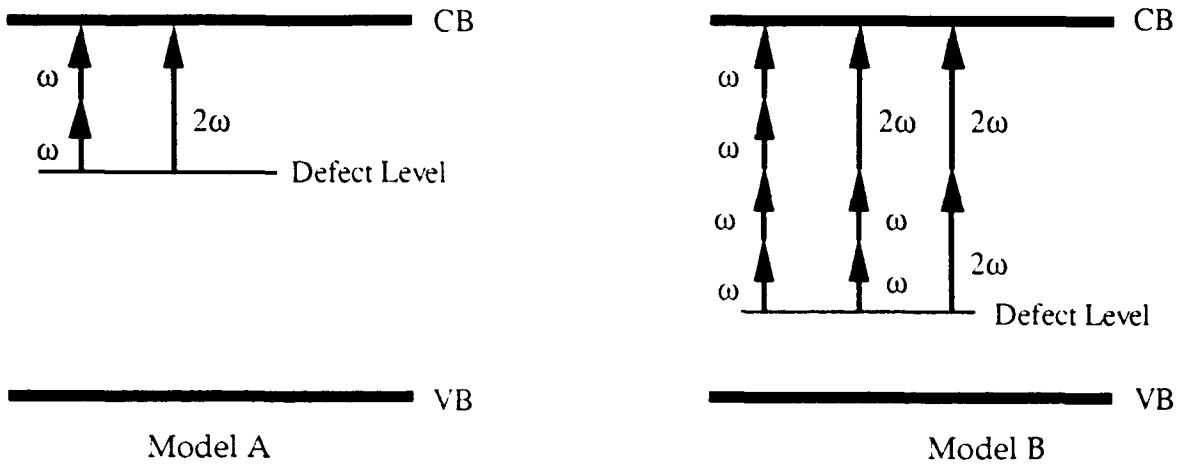

Figure 1) Energy level model associated with anisotropic photoelectron emission from germanium-doped fused silica. Model A is the simple picture, however there is very little absorption at λ=532 nm in the glass materials generally used for these experiments. In model B there are three separate ionization channels that interfere. The defect level is associated with the known λ=240 nm absorption band in germanium-doped glass.

model B applies to germanium-doped glass systems (which includes most communication optical fibers and preforms), we expect the second-harmonic generation effect to be strongly intensity dependent, due to the multi-photon nature of the ionization. Consequently, the second major thrust of the research performed under this JSEP fellowship was to measure the intensity dependence of this effect to see if it fit model B. We found that the intensity dependence was even stronger than expected from model B,[16] and that the photo-ejection of electrons is more complicated than predicted by this simple model. In particular we found evidence that other energy levels (metastable) of the glass system are involved. Our paper describing this work[6,7] has been accepted for publication in Optics Letters (see Appendix A).

3) SUMMARY OF RESULTS

There are three important conclusions from our work:

* Experiments involving second-harmonic generation in glass are simpler and easier to interpret if they are performed in bulk glass samples rather than in optical fibers.

We used optical fiber preform samples made from the same glass as the communication fibers used by most researchers.

* The creation of the second-order nonlinearity inside the glass can be completely explained by invoking a DC electric field $\vec{E}_{dc}$. Thus, the following equation explains the induced nonlinearity:

$$\vec{\vec{\chi}}^{(2)}(-2\omega;\omega,\omega) = 3\,\vec{\vec{\chi}}^{(3)}(-2\omega;\omega,\omega,0)\cdot\vec{E}_{dc}.$$

* The mechanism that induces the DC electric field definitely involves multi-photon interactions. This is demonstrated by our measurement of the intensity dependence of the rate-of-formation of the DC field. It seems likely that interference of multi-photon ionization channels in the presence of a laser beam (E_ω) and its second harmonic ($E_{2\omega}$) produces an anisotropic distribution of ejected electrons, which can be thought of as a photogalvanic current. This current builds up the DC electric field $\vec{E}_{dc}$.

4) ADVANTAGES OF BULK GLASS SAMPLES OVER OPTICAL FIBERS

We began our studies of second-harmonic generation using optical fibers. However, after struggling for about a year and a half to obtain reproducible results, we switched to experiments in bulk glass samples. Our bulk glass sample is an optical fiber preform. Optical fiber preforms are carefully grown cylindrical glass rods which are later heated to the melting point and drawn into optical fibers. For the purposes of our experiments, the bulk glass preform is equivalent to an optical fiber. There are minor differences in the glass structure of a fiber versus a preform, such as the number density of certain kinds of defects,[19] however we don't expect this to adversely affect the applicability of our results. There are definite advantages to using bulk glass samples over fibers for these experiments. These advantages made it possible to carry out reproducible, well-controlled experiments. I list below the major advantages.

Elimination of modal overlap problems

Only certain spatial distributions of light (modes) can propagate in an optical fiber, and this causes problems. For example, in our experiments we need to inject two different

color light beams, one at frequency ω and one at frequency 2ω, and the allowed modal shapes for the two different colors will be different in a fiber. Even if a fiber is single mode at ω, in general it will be multi-mode at 2ω. This means that the spatial overlap of the two optical fields (E_ω and $E_{2\omega}$) will change if the coupling into the optical fiber changes or if the fiber is perturbed by the slightest vibration or bend. Consequently, the spatial overlap depends on the exact launching conditions into the fiber, and can change from one experiment to the next, or even during a single experiment. Because the modal overlap of the launched E_ω and $E_{2\omega}$ fields is difficult to control, it makes it quite difficult to obtain consistent, reproducible experimental results. There is one remedy for this situation: use a fiber that is single mode at both ω and 2ω. However, in this case the fundamental (E_ω) wavelength is only weakly guided and the majority of its energy actually propagates in the cladding region of the fiber. This loss of power in the core of the fiber greatly reduces the rate at which electrons are ejected in the fiber, and it also makes it tricky to determine the amount of power actually contained in the core, because power measurements are easily polluted by light propagating down the fiber in so-called "cladding modes." In the case of such weak guiding, the fundamental optical field is also quite susceptible to bending-induced out-coupling, so that small vibrations cause the light to leave the optical fiber core and radiate away. Because of the complications caused by the use of a fiber that is single mode at both ω and 2ω, only one experiment has been reported to date in such a fiber.[10]

Another restriction imposed by the discrete modes of an optical fiber, and which is absent in a bulk sample, is the spatial shape of the generated second-harmonic signal. I will report later in this document how the spatial shape of the generated second-harmonic beam can give very useful information about the shape of the internal DC electric field. Such experiments would be impossible in an optical fiber, for not only is the spatial shape of the generated signal restricted to the allowed modes of the fiber, but also the fiber geometry does not allow one to probe the induced field $\vec{E}_{dc}$ at any other point except at the center of the fiber. This means that in a fiber one cannot map the shape of the induced DC field by translating a probe beam, as we can in bulk glass samples, as we describe in Section 5 below.

Elimination of de-phasing problems

Since we must focus rather tightly into a bulk glass sample to achieve the same optical intensities as exist in optical fibers, we have correspondingly short interaction lengths. This means that the measured second-harmonic signal will be weak. However, the reduced interaction length (200 μm versus 20 cm) means that the interaction will be about 100 times less sensitive to dephasing effects. There are several important dephasing mechanisms, including self-phase modulation, cross-phase modulation, and temperature-induced changes in the refractive index; all of these effects were found to be present in our experiments with optical fibers and absent in our experiments with bulk glass.

Various other advantages

Another major advantage of bulk samples is that, once they are cut and polished, it is possible to perform many independent experiments in different regions of the sample before it is necessary to switch to a new sample. This is not true of optical fibers, which *must be discarded after each* experiment. This means that exorbitant amounts of time are spent on fiber preparation and alignment. Also, because the required intensities are very near the damage threshold of fused silica, the input cleave of a fiber is frequently damaged. In a bulk sample, if a region becomes damaged one simply translates the sample away from the damage spot. Also, at low intensities the rate-of-formation becomes very slow (hours), and it is difficult to maintain coupling stability into a fiber for such extended times.

In all fairness, there are two drawbacks to using bulk samples which should be pointed out. First, their relatively short interaction length limits the generated second-harmonic signal to quite small values, such that sensitive detectors (PMTs) and electronics must be used. This is not a major difficulty. Second, precise spatial overlap of the fundamental and second-harmonic seeding beams requires that special optics be used to focus the laser into the sample. This is a rather tricky experimental point which is not widely appreciated.

5) ELECTRIC-FIELD INDUCED SECOND-HARMONIC GENERATION

Mizrahi *et al.* showed in 1990 that the polarization properties of the induced nonlinearity could be completely explained by invoking the known nonlinear susceptibility $\chi^{(3)}$ tensor of glass and a single cartesian component of the induced DC electrical field.[10] Their experiments were carried out in a fiber that was single mode at both the fundamental (ω) and the second-harmonic frequency (2ω). They seeded the sample with both beams polarized vertically, which should cause charges to be separated vertically by the photogalvanic current. To explain their observations, Mizrahi *et al.* needed only to invoke the vertical component of the DC electric field. There are two reasons for this: 1) They can only launch light into the core of the optical fiber, and since this is the point of symmetry for the vertical charge separation, the field is mostly vertically oriented in this region. 2) The symmetry of the horizontal component of the DC electric field is such that it will generate a four lobed mode that is not an allowed propagation mode in this fiber. (Thus the single-mode nature of the fiber prevents determination of the shape of the DC electric field.)

We have extended the work of Mizrahi *et al.* by performing similar experiments in bulk glass samples.[12] In the bulk sample we are free to probe the induced field at whatever point we choose merely by translating a probe beam. Also, the shape of the generated second-harmonic signal is not constrained. We performed two independent experiments to determine the shape of the induced electrical field. In the first experiment we seeded the bulk sample with an actively mode-locked (76 MHz, 100 ps FWHM), Q-switched (1 kHz, 300 ns FWHM) laser beam which was doubled in a temperature-tuned, non-critically phase-matched crystal of LBO ($LiBO_3$). The average power in the infrared (1.064 μm) was typically 4 W and in the green (0.532 μm) was ~2 mW. Both colors were focused to the same location inside the sample with a 5X lens designed specifically to be achromatic at these two wavelengths. The infrared and green beams had $1/e^2$ of intensity radii of ~9 μm and ~7.5 μm, respectively. The sample was seeded for 3 minutes, during which time the generated second-harmonic signal was monitored until it reached a nearly saturated level. Both laser beams were vertically polarized during seeding. After 3 minutes, we blocked the seeding green beam and decreased the infrared power so that no further change was induced inside the glass. We inserted a $\lambda/2$ waveplate (@ 1.064 μm) immediately before the focusing achromat

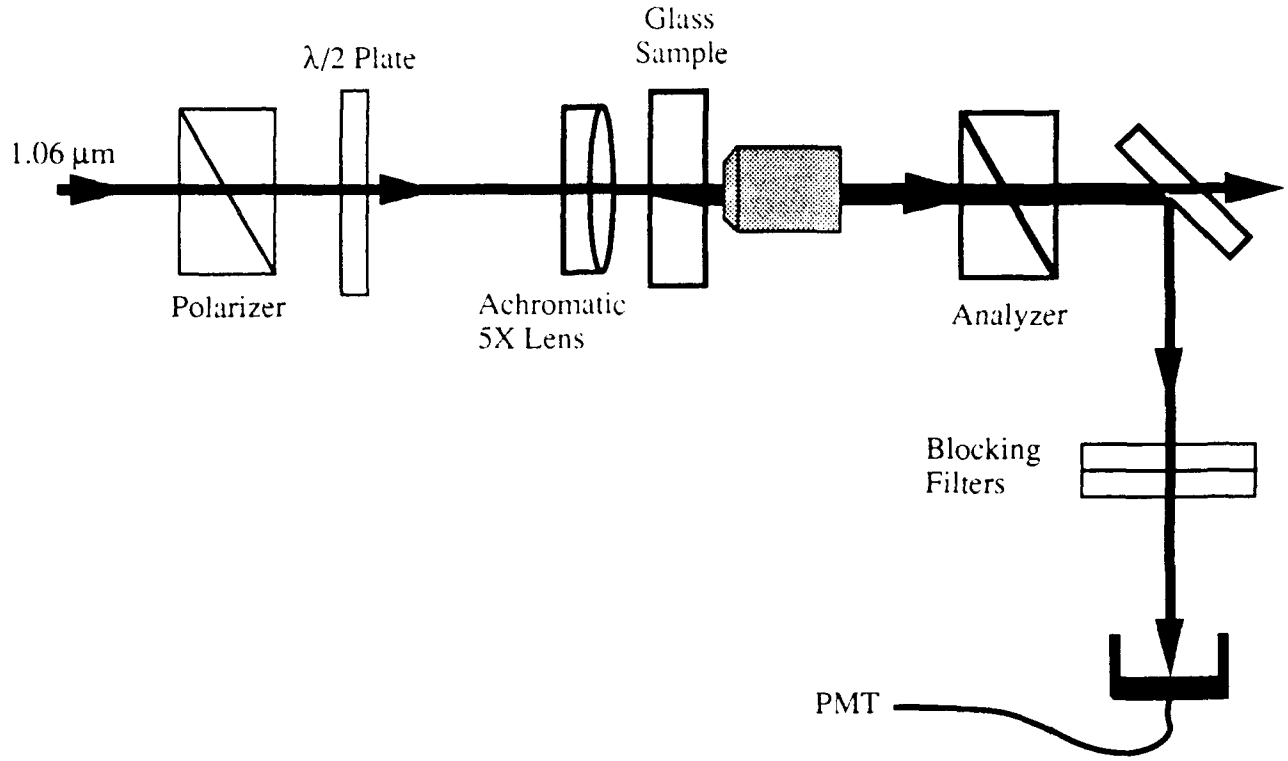

Figure 2) Experimental setup to map out the transverse dependence of the induced DC electric field inside a glass optical fiber preform.

and an analyzer after the collecting objective (see Fig. 2), so that we could control the input infrared reading polarization and the detected signal polarization. The generated signal was proportional to:

$$I_{2\omega} \propto \left| \hat{e}^{*}_{analyzer} \cdot \left(\vec{\vec{\chi}}^{(3)} : \vec{E}_{\omega}\, \vec{E}_{\omega}\, \vec{E}_{dc} \right) \right|^2 \qquad (2)$$

where $\vec{E}_{\omega}$ is the infrared probing beam, $\vec{E}_{dc}$ is the DC electric field and $\hat{e}_{analyzer}$ is the unit vector describing the orientation of the analyzer. Because of the symmetry of $\chi^{(3)}$ in glass, if we vertically polarize the probe beam and we set the analyzer to vertical then only the vertical component of $\vec{E}_{dc}$ can contribute to the measured signal. Thus, if we move the probe beam around we can map the strength of $\left|\hat{y} \cdot \vec{E}_{dc}\right|^2$ as a function of transverse position. We can also perform the complementary experiment in which the probe beam is horizontally polarized and the analyzer is horizontally oriented. This

maps the horizontal component $\left|\hat{x}\cdot\vec{E}_{dc}\right|^2$ of the DC electric field. We take the square root of such data to obtain a map of the two transverse components of the DC field. To turn this information into a vector map of the field we need to perform a separate experiment to determine the relative sign between the vertical and horizontal field components. We determine the relative phase between the transverse field components by rotating the input probe polarization with a fixed analyzer (either vertical or horizontal). The shape of the signal as the input polarization is rotated determines whether the product $E_{dc}^{hori}\,E_{dc}^{vert}$ is positive or negative.

There is a complication to this experiment. Since the probing beam was not infinitely small we actually average the strength of $\left|\hat{y}\cdot\vec{E}_{dc}\right|^2$ and $\left|\hat{x}\cdot\vec{E}_{dc}\right|^2$ over the area of the probing beam, which smears out the information. Also, since the sign of the term $E_{dc}^{hori}\,E_{dc}^{vert}$ may be different in different regions of the probed area, we cannot uniquely assign either a positive or a negative sign to this term. A simple way to overcome this difficulty is to allow the $E_{dc}^{hori}\,E_{dc}^{vert}$ term to be complex (neither fully positive or negative). This works wonderfully. In this case, the cross-product term $E_{dc}^{hori}\,E_{dc}^{vert}$ may be assigned a relative phase o which enters the prediction for the measured signal only as cos[o]. If $o>\pi/2$ then the cross-product term is more negative than positive, and the opposite is true if $o<\pi/2$. In this way we can use our experiments with the rotating probe polarization to determine the relative sign between the vertical and horizontal DC field components in the glass caused by its previous irradiation by light beams.

Here are our results. We first assume a shape for the transverse distribution of charge. This charge distribution is assumed to be:

$$\rho(x,y) \;=\; -\rho_0\, y \exp\left[-\frac{x^2+y^2}{(5\,\mu m)^2}\right] \qquad (3)$$

which is simply the y-derivative of a cylindrically symmetric gaussian. This leads to the field distribution shown in Fig. 3. We wrote a simple computer program to predict how the measured second-harmonic signal should vary as the probe beam location is varied. This program assumed that the DC electric field was as shown in Fig. 3, and it took into account the finite size of the probing beam. Figures 4 and 5 show a comparison of the

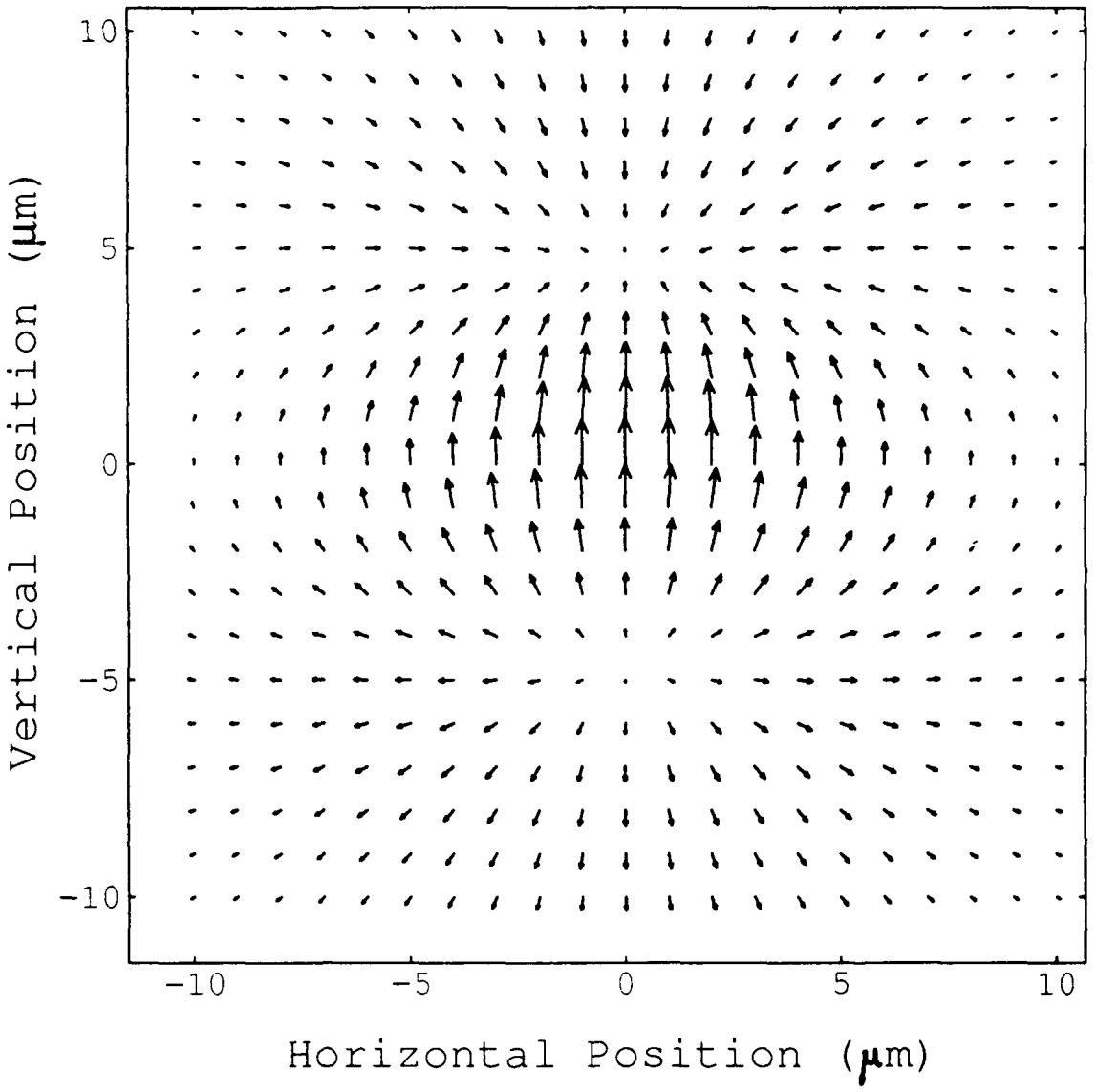

Figure 3) This is the DC electric field of the charge distribution given by Eq. (3) in the text. This electric field is used to predict the results of two separate experiments in our bulk glass samples.

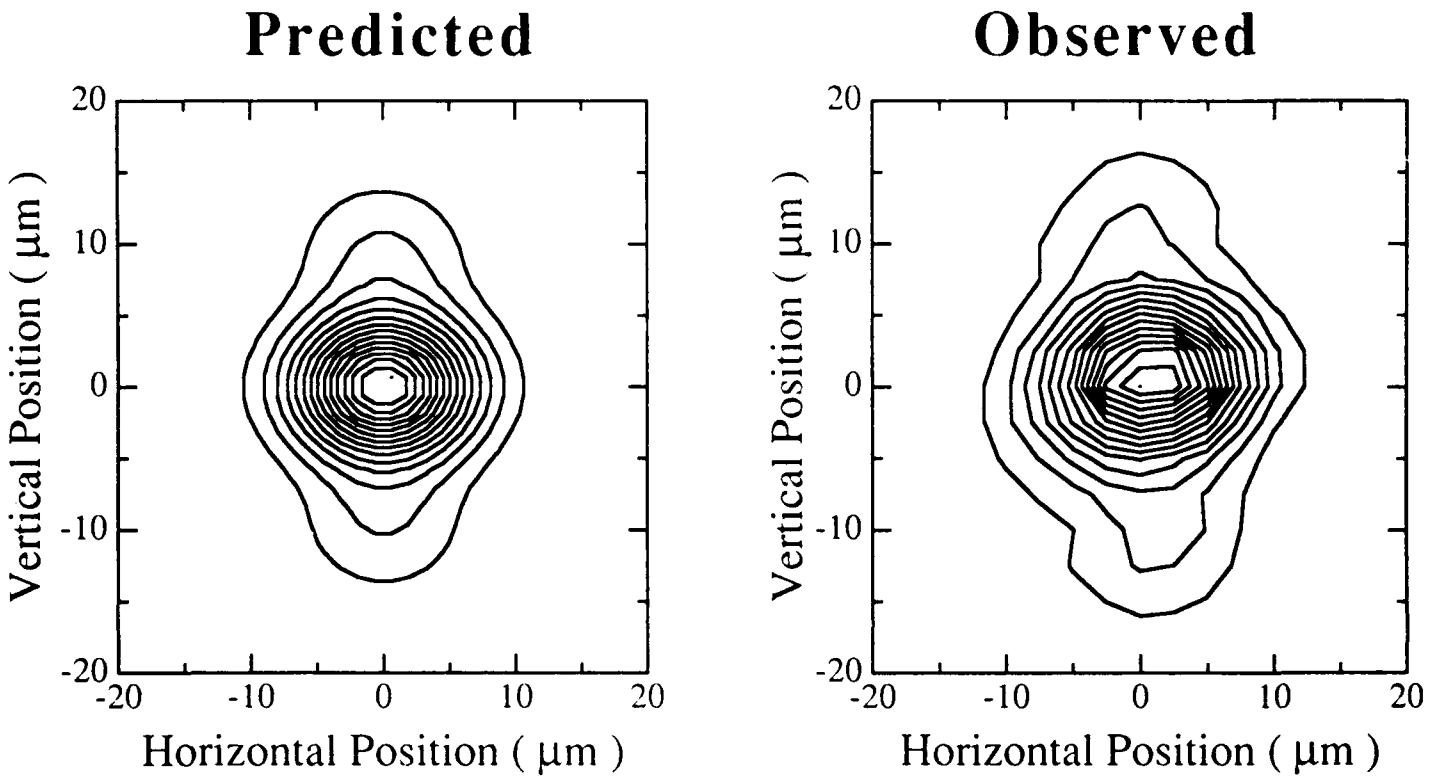

Figure 4) Comparison between the theoretically predicted and the experimentally observed second-harmonic signal versus position of the probing beam. The polarization of the probing beam is vertical and the analyzer passes only vertically polarized light. These graphs show contour plots of equal signal strength. The strength of the contour values increase monotonically towards the center of the graphs. The wings on the top and bottom of the contour maps correspond to regions where the vertical component of the DC electric field switches sign. The theoretical map was generated using the DC electric field shown in Fig. 3 and the known 9 μm radius of the probing beam.

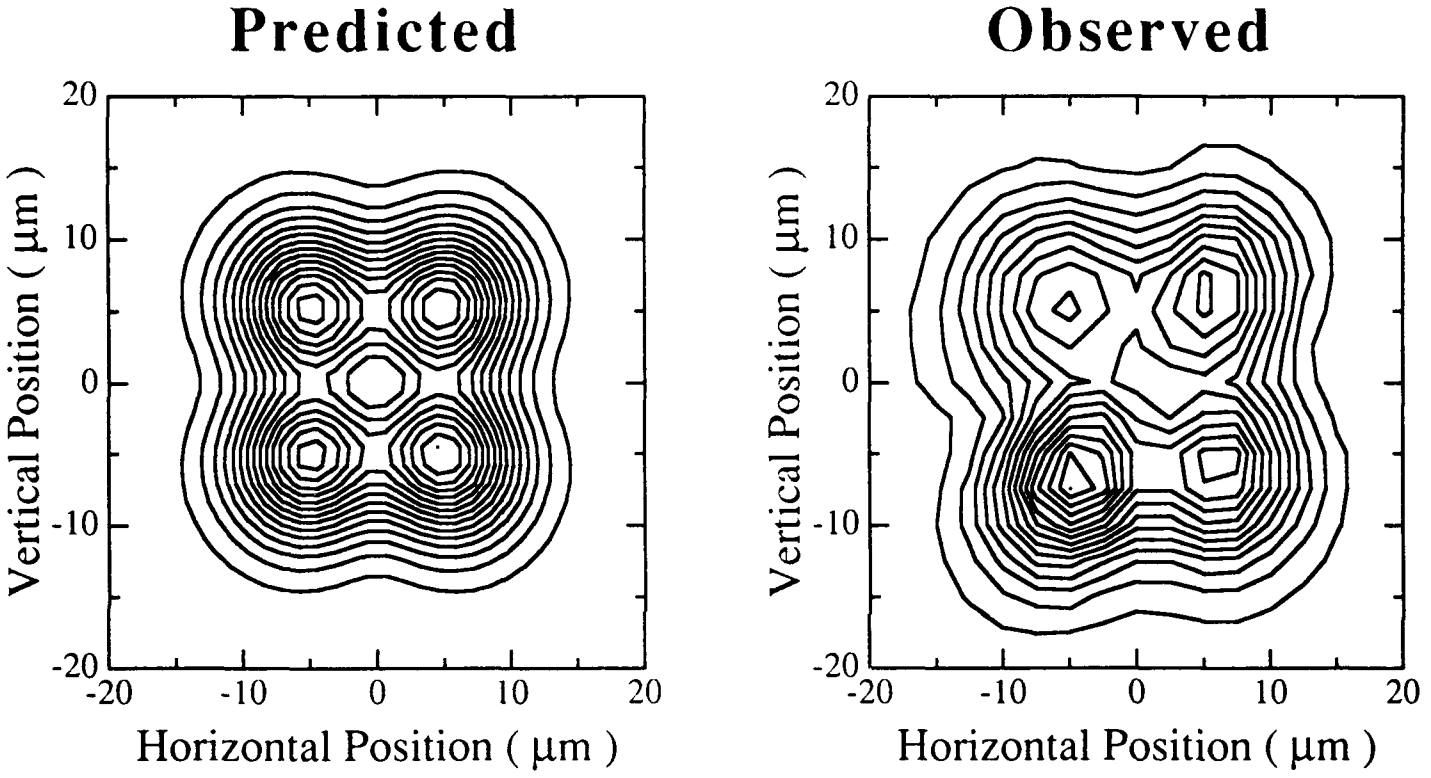

Figure 5) Same as Fig. 4 except now the probing light is polarized horizontally and the analyzer is set to pass horizontally polarized light. In this case the contour plots show a four-lobed pattern. (With a much smaller probing beam the signal would drop to zero between each of the four peaks.) The slight asymmetry in the experimental data is attributed to imperfect overlap of the fundamental and second-harmonic seeding beams. The theoretical map was generated using the DC electric field shown in Fig. 3 and the known 9 μm radius of the probing beam.

predicted and observed dependence of the strength of the generated second-harmonic signal as the position of the probing beam is translated. Figure 4 shows the case where the probe polarization is vertical, the analyzer orientation is vertical, and the preform sample was translated side to side and up & down to map out the spatial dependence. Figure 5 gives the corresponding comparison for the horizontal input polarization/horizontal analyzer case. The comparison was quite good. However there was a significant amount of smearing of the spatial information because of the large probe beam size. This is especially obvious in Fig. 5. When we rotated the probe polarization with a fixed analyzer to determine the sign of $E_{dc}^{horz}\,E_{dc}^{vert}$ in each of the four quadrants, we confirmed that the DC field components have the relative sign shown in Fig. 3. In brief, then, these experiments confirm that the induced DC electric field looks like the field shown in Fig. 3. The asymmetry in the observed data of Fig. 5 is thought to arise from the slightly imperfect spatial overlap of the infrared and green seeding beams.

We also performed an independent experiment to confirm that the DC field had the assumed shape. We observed the spatial shape of the generated second-harmonic signal as the probe polarization is rotated, as first suggested by Driscoll and Lawandy.[20] We observed the signal's mode shape using either a vertical or horizontal analyzer, as shown in Fig. 6. For this experiment we would prefer to have an infinitely big probing beam. However, since this is not feasible we can use the same computer program discussed previously to take into account the finite size of the reading beam. The program predicted how the far-field mode shape should vary with the reading polarization.

We made a video which shows a side-by-side comparison between our computer prediction of the far-field mode shape and the actually observed mode shape dance. We animated the computer prediction and recorded the computer screen. We then used the setup shown in Fig. 6 to film the observed signal on the CCD camera. In both cases, using either a vertically or a horizontally oriented analyzer, the agreement between the prediction and the observation was quite good. This video premiered at the Optical Society of America Annual Meeting in September 1992, and is available upon request.

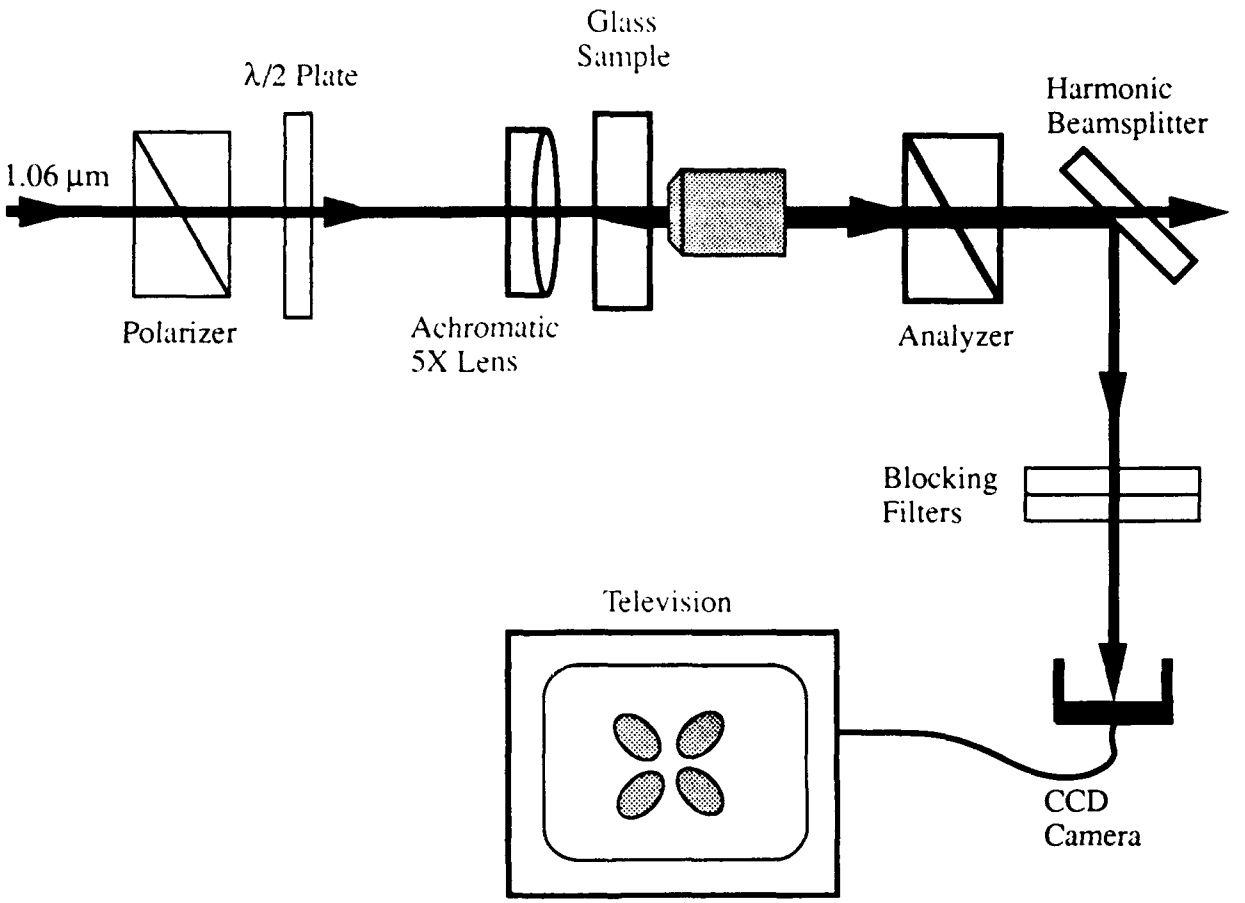

Figure 6) Experimental setup to observe the far-field spatial mode pattern of the generated second-harmonic signal. The analyzer is set to pass either vertically or horizontally polarized light, and the input polarization is continuously rotated using a λ/2 plate mounted on a motorized rotation stage. The mode pattern is viewed with a CCD camera and a television monitor.

Two independent experiments confirm that the induced electric field looks as shown in Fig. 3. We consider this a complete verification of the predictions of Eq. (1) above. We now have no doubt that second-harmonic generation in glasses is caused by a DC electric field inside the material.

6) MULTI-PHOTON NATURE OF DC FIELD FORMATION MECHANISM

We have performed extensive measurements of the rate-of-formation of the DC electric field in a germanium-doped optical fiber preform. We presented this work at CLEO

1992 (Ref. 6) and we expect it to be published in Optics Letters soon (Ref. 7). Since our submission to Optics Letters contains all the pertinent details, I include a pre-print of this paper here as an appendix.

7) LIST OF PUBLICATIONS

1. Vince Dominic, X. S. Yao, R. M. Pierce, and Jack Feinberg, "Measuring the coherence length of mode-locked laser pulses in real time," Appl. Phys. Lett. **56**, 521-523 (1990).
2. X. Steve Yao, Vince Dominic, and Jack Feinberg, "Theory of beam coupling and pulse shaping of mode-locked laser pulses in a photorefractive crystal," JOSA B **7**, 2347-2355 (1990).
3. Vince Dominic and Jack Feinberg, "Intensity dependence of second-harmonic generation in germanium-doped fiber preforms," in *Conference on Laser and Electro-Optics 1992*, (Optical Society of America, Washington, DC 1992), paper JTuA5.
4. Vince Dominic and Jack Feinberg, "Growth rate of second-harmonic generation in glass," accepted for publication in Optics Letters.
5. Vince Dominic and Jack Feinberg, "Spatial mapping of the DC electric field induced in optical fiber preforms by intense light," in *Digest of Optical Society of America Annual Meeting* (Optical Society of America, Washington, DC 1992), paper TuB4.

8) ADVANCED DEGREES EARNED

Mr. Dominic expects to complete his Ph.D. in the spring of 1993. He gratefully acknowledges that the JSEP fellowship made this research possible, and will continue to cite gratitude to the JSEP for work which was begun during the tenure of his JSEP fellowship.

9) REFERENCES

1. Vince Dominic, X. S. Yao, R. M. Pierce, and Jack Feinberg, Appl. Phys. Lett. **56**, 521-523 (1990).
2. X. Steve Yao, Vince Dominic, and Jack Feinberg, JOSA B 7, 2347-2355 (1990).

3. X. Steve Yao, "Optical pulse coupling in a photorefractive crystal, propagation of encoded pulses in an optical fiber, and phase conjugate optical interconnections," Ph.D. Thesis, University of Southern California (1992).
4. U. Österberg and W. Margulis, Opt. Lett. **11**, 516-518 (1986); Opt. Lett. **12**, 57-59 (1987).
5. N. M. Lawandy and M. D. Selker, Opt. Commun. 77, 339-342 (1990); M. D. Selker and N. M. Lawandy, Opt. Commun. 81, 38-42 (1991).
6. Vince Dominic and Jack Feinberg, in *Conference on Laser and Electro-Optics 1992*, (Optical Society of America, Washington, DC 1992), paper JTuA5.
7. Vince Dominic and Jack Feinberg, accepted for publication in Optics Letters.
8. Y. R. Shen, The Principals of Nonlinear Optics (Wiley, New York, 1984), Chap. 2, p. 28.
9. R. H. Stolen and H. W. K. Tom, Opt. Lett. **12**, 585-587 (1987)
10. V. Mizrahi, Y. Hibino, and G. Stegeman, Opt. Commun. **78**, 283-288 (1990).
11. A. Kamal, M. L. Stock, A. Szpak, C. H. Thomas, D. A. Weinberger, M. Frankel, J. Nees, K. Ozaki, and J. Valdmanis, in *Digest of Optical Society of America Annual Meeting* (Optical Society of America, Washington, DC 1990), paper PD25.
12. Vince Dominic and Jack Feinberg, in *Digest of Optical Society of America Annual Meeting* (Optical Society of America, Washington, DC 1992), paper TuB4.
13. P. N. Butcher and D. Cotter, The Elements of Nonlinear Optics (Cambridge University Press, Cambridge, 1990), Chap. 2, pp. 24-27.
14. E. M. Dianov, P. G. Kazansky, and D. Yu Stapanov, Sov. J. Quantum Electron., **19**, 575-576 (1989).
15. N. B. Baranova, A. N. Chudinov, and B. Ya. Zel'dovich, Opt. Commun. **79**, 116-120 (1990).
16. D. Z. Anderson, V. Mizrahi, and J. E. Sipe, Opt. Lett. **16**, 796-798 (1991).
17. N. B. Baranova, I. M. Beterov, B. Ya. Zel'dovich, I. I. Ryabtsev, A. N. Chudinov, and A. A. Shul'ginov, JETP Lett. **55**, 439-444 (1992).
18. A. V. Smith, Y. Yin, C. Chen, and D. S. Elliott, in *Bulletin of the American Physical Society* **37**, 1207 (1992), paper TuM5.
19. Y. Watanabe, H. Kawazoe, K. Shibuya, and K. Muta, Jap. J. of Appl. Phys. **25**, 425-431 (1986).
20. T. J. Driscoll and N. M. Lawandy, in *Conference on Laser and Electro-Optics 1992*, (Optical Society of America, Washington, DC 1992), paper JTuA4.

Growth rate of second-harmonic generation in glass

Vince Dominic and Jack Feinberg

Departments of Electrical Engineering and Physics, University of Southern California, Los Angeles, CA 90089-0484

We study the growth rate of the light-induced second-order nonlinearity in germanium-doped optical fiber preforms. We seed the glass with both infrared light and green light (Nd:YAG and doubled Nd:YAG) to create the second-order nonlinearity, and measure its formation rate while varying the intensity of either the fundamental or second-harmonic seeding beams. We find that the formation rate varies as a power law of the intensities, but with an exponent larger than predicted by recent models.

Because the core of an optical fiber is macroscopically centrosymmetric, two-wave sum frequency generation (and in particular second-harmonic generation) is not expected to occur. However, in 1987 Österberg and Margulis reported rather efficient (5%) second-harmonic generation of 1.064 μm light inside a germanium-doped optical fiber that had been illuminated by intense infrared light for many hours.[1] Stolen and Tom[2] showed that by injecting both infrared and green light into the fiber, the preparation time of the fiber could be shortened from many hours to just a few minutes.

What breaks the inversion symmetry of the glass? Recent experiments indicate that the incident light gradually produces a spatially periodic[3] DC electric field in the glass.[4,5] This DC electric field induces a second-order nonlinearity:

$$\chi^{(2)}(-2\omega;\omega,\omega) = 3\chi^{(3)}(-2\omega;\omega,\omega,0)E_{dc}. \quad (1)$$

Phase-matching can be achieved if the DC field (E_{dc}) periodically changes direction along the fiber length. Many theories have been postulated to explain the origin of this spatially periodic DC electric field.[2,6-9] However, these different models predict different dependencies of the growth rate of the DC field on the intensity of the injected optical beams. To discriminate among these models we measured the dependence of the growth rate of the second-harmonic signal on the intensity of the injected light beams.

We found it simpler to perform our experiments in glass fiber preforms instead of in the fibers themselves. Our preform sample had an outer diameter of 12.5 mm and a 3.4 mm diameter germanium-doped core.[10] The germanium concentration decreased abruptly at the core-cladding interface and then fell exponentially with distance, with occasional rings of higher index. These rings result from the fabrication process, and they aberrate optical beams transmitted through them. We performed our experiments far enough away from the core to avoid these aberrations. We worked in the cladding region so that we could fit many more experiments into one rotation of the sample. We verified that the dependence of the growth rate on intensity was the same in the core region as in the cladding region of the preform. Before starting each experiment we rotated the sample to a new, unused portion of the preform. Because the doping was cylindrically symmetric, the germanium density remained constant from experiment to experiment.

We used a seeding technique[2] in which we focused both the fundamental and some externally generated second-harmonic light into the sample. (In the absence of a second-harmonic seeding beam no second-harmonic generation was observed from the preform.) A mode-locked and Q-switched Nd:YAG laser [Coherent Antares] had a Q-switch repetition rate of 1 kHz, with ~23 mode-locked pulses under the 300-ns Q-switch pulse envelope. Its 1.064 μm light was doubled in a non-critically phase-matched LBO crystal to produce second-harmonic light colinear with the fundamental light. We controlled the power levels of the fundamental and second-harmonic seeding beams independently with two harmonic waveplates. The paths of our seeding fundamental (I_ω) and second-harmonic ($I_{2\omega}$) beams were never separated to ensure that their relative phase remained stable during seeding.[11] We checked this phase stability and found that it exceeded four hours.

A spinning wheel (~5 Hz) in front of the sample periodically and momentarily blocked the green seeding beam (with both a cold mirror and an RG780 absorption filter), so that any green light generated in the sample could be measured. Light reflected from the cold mirror was used to trigger the data acquisition system. The power in each incident infrared and green pulse was monitored with photodiodes, and the generated green light was monitored with a photomultiplier. All of these detectors were carefully checked for linearity over their range of detected intensities. A 25 mm focal length achromatic lens focused the infrared and the green to the same location within the glass preform. The infrared and green beams were measured to be 9.7 μm and 7.4 μm (radius at $1/e^2$ of intensity), respectively, at the focus.

We acquired two types of data sets: 1) we held the infrared power constant and varied the green power level, or 2) we held the green constant and varied the infrared power level. For both types of experiments, we measured the early time growth of the second-harmonic signal and fit its dependence to a quadratic function of time, as shown in Fig. 1. We fit the data up to the point where it began to saturate, i.e. where the growth was no longer quadratic in time, which could take longer than 40 minutes at low infrared and green intensities. We performed fits using two different fitting functions:

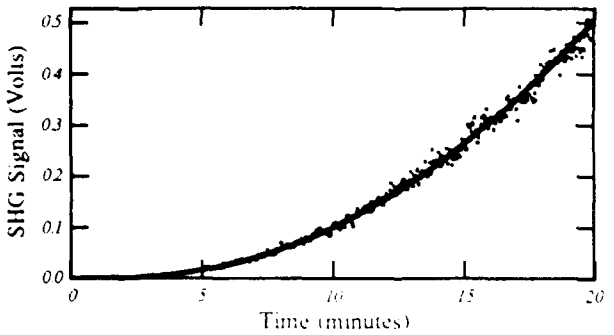

Fig. 1. Quadratic growth of the second harmonic signal during seeding. The solid line is a fit using Eq. 3. The inset shows the same data plotted log-log with the best fit using Eq. 2 (dashed) and using Eq. 3 (solid).

$$I_{2\omega}^{produced} = \Gamma t^2 + \text{offset} \qquad \text{or} \qquad (2)$$

$$I_{2\omega}^{produced} = \Gamma[t - \tau(1-\exp(-t/\tau))]^2 + \text{offset}, \qquad (3)$$

where "offset" is a small DC voltage produced by our detection system. We found that Eq. (3) fit the data better than Eq. (2), especially at early times, as shown in the inset of Fig. 1. We derived Eq. (3) by assuming an initially unoccupied level must first be populated (with a time constant τ) before the internal DC electric field can begin to form. This idea was inspired by recent suggestions that metastable levels may be involved in the induced second-harmonic generation effect.[12,13] We found experimentally that τ varied from 3 minutes at low intensities to less than a second at high intensities.

For all feasible power levels, we determined the growth rate Γ and then fit it to a power law in the optical intensities: either AI_ω^x for the infrared or $BI_{2\omega}^y$ for the green. Figure 2 shows the dramatic variation of Γ with the infrared seeding intensity and the less dramatic variation of Γ with the green seeding intensity. Figure 3 shows the results of accumulating many such power law dependencies; we plot the exponent x in $\Gamma = AI_\omega^x$ as a function of the green seeding intensity in Fig. 3a, and the exponent y in $\Gamma = BI_{2\omega}^y$ vs. the infrared seeding intensity in Fig. 3b. We found that the exponent y varied from y=3.5 at low infrared intensity to y=2.5 at high infrared intensity. In contrast, the exponent x varied from x=12.5 at low green seeding intensity to x=8 at high green seeding intensity.

How do our data compare with the current theories of second-harmonic generation? The models of Dianov *et al.*[8] and Anderson *et al.*[9] postulate a spatially oscillating photogalvanic (j_{pg}) current to explain the generation of the DC electric field. At early times the current flows unchecked and the DC electric field grows linearly in time: $E_{dc} \propto j_{pg}\, t$. In our experiments we measured the second-harmonic signal power, which is proportional to $|\chi^{(2)}|^2$ of Eq. (1), so that according to the photogalvanic current models[8,9], we measured $|j_{pg}|^2$. The predicted intensity dependencies for our parameter Γ from the model of ref. [8] is then:

$$\Gamma \propto \left\{ I_{2\omega}\, I_\omega^2 \right\} I_\omega^2 \qquad (4)$$

while from the model of ref. [9] it is:

$$\Gamma \propto \left\{ I_{2\omega}\, I_\omega^2 \left[\eta_3^2\, I_\omega^4 + \eta_4\, I_\omega^2\, I_{2\omega} + I_{2\omega}^2 \right] \right\} I_\omega^2. \qquad (5)$$

In Eqs. (4) and (5) the terms inside the braces are proportional to $|j_{pg}|^2$, while the reading process itself imparts the additional quadratic variation (I_ω^2) to the measured growth rate Γ. This extra quadratic variation is *not* normalized out of the data displayed in Figs. 2 and 3. If we include this built-in quadratic dependence on I_ω, then the anisotropic photoionization model[9] predicts a power law $\Gamma \propto I_\omega^x$ with the exponent ranging from x = 4–8. Another model[8] gives x = 4. The trend in Fig. 3 is consistent with the model of Anderson *et al.*, in that the power law exponent drops to a lower value as the green seeding intensity is increased. However, even at the highest obtainable green intensity we still observe x=8. This data clearly indicates a higher-order dependence on I_ω than predicted by either model.

There have been previous reports[14–16] of the intensity dependence of seeded second-harmonic generation in germanium-doped fused silica. Kamal *et al.*[16] performed experiments quite similar to the ones reported here, however their experiments were carried out in a specially grown fiber. If their data are analyzed using the growth rate parameter Γ discussed here, then they observed $x \approx 4$ for the dependence of the rate on infrared intensity, and $y \approx 3$ for the dependence on green intensity. Their observed dependence of the rate on the green intensity agrees with ours, but their infrared dependence is quite different.

Lawandy and Selker[15] reported a distinct infrared intensity threshold below which no second-harmonic generation was observed in samples that had been seeded for only 20 minutes. Our data also shows a very dramatic dependence

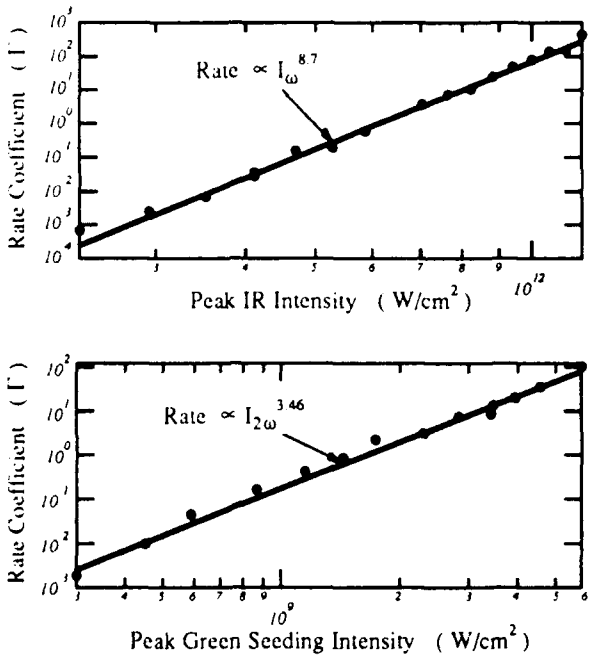

Fig. 2. (a) Dependence of the rate Γ on the infrared seeding power, with the green seeding power held fixed at 6 mW. (b) The dependence of the rate Γ vs. the green seeding power, with the infrared power held constant at 3 W.

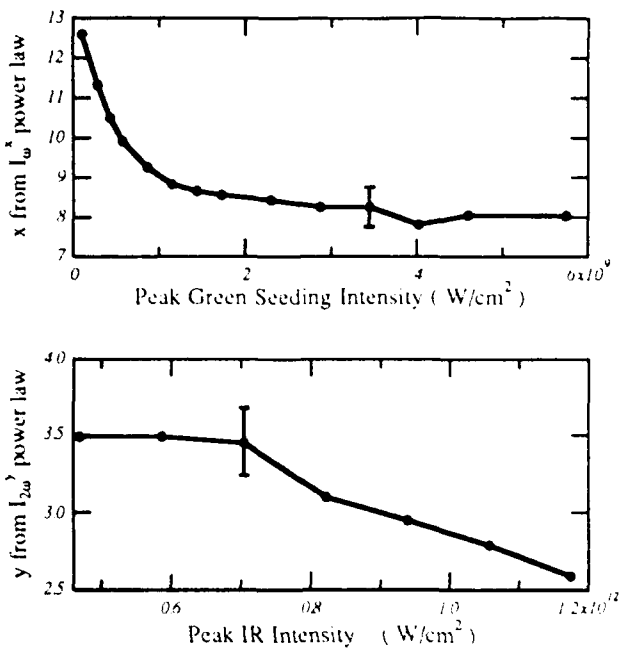

Fig. 3. (a) Dependence of the infrared power law exponent "x" on the green seeding set-point intensity. (b) Dependence of the green power law exponent "y" on the infrared set-point intensity.

of the second-harmonic effect with the infrared intensity, but at intensities 100 times greater than the threshold cited in ref. [15]. Rather than observe a threshold intensity below which no effect occurs, we find that at low infrared intensities the formation rate of the DC electric field simply becomes extremely slow.

Our observed green intensity scaling data are not in gross disagreement with the anisotropic photoionization model of Anderson *et al.*[9] However, the infrared scaling data requires more infrared photons than this model postulates. We examined our experiment to see if systematic errors caused the higher-than-expected I_ω variation. First we checked whether the beam spot size entering the focusing lens changed as we adjusted the infrared power. We measured the infrared beam profile and found no systematic variation of the beam width to within experimental error (0.6%). Additionally, we checked to see if self-focusing or thermal lensing changed the focal spot size as the power was varied and we found no variation. We intentionally displaced the infrared beam from the green seeding beam by ~6 μm at the focus to determine whether thermal beam steering contributed to the intensity dependence, and found that although the infrared power law exponent "x" was lower with the beams offset, it was still within the error bar of Fig. 3a.

Because the diameters of our tightly focused optical beams change as they propagate through the glass preform, their intensity varies in both the transverse directions and along the propagation direction and therefore so should the growth rate. However, we performed numerical calculations and found that the measured signal should still grow quadratically in time. Because only the most intense part of the beam contributes to the signal at early times, the intensity scaling laws of the early time growth rate are not affected. Another complication is that our laser is Q-switched and mode-locked, so that there is a range of peak intensities present under the envelope, and our measured rate is an average over all of these peak intensities. This averaging over intensities could mask an even more dramatic dependence of the generation rate on optical intensity.

In summary, we measured the buildup rate of the second-harmonic signal in germanium-doped fused silica optical fiber preforms. The second-harmonic signal rises quadratically in time. The rate coefficient increases with the intensity of the infrared seeding beam as I_ω^{8-12}, and with the intensity of the green seeding beams as $I_{2\omega}^{2.5-3.5}$. Both the I_ω and $I_{2\omega}$ power laws are faster then predicted by the model of Dianov *et al.*[8] The variation of the rate with the intensity of the green seeding light seems to agree with the model of Anderson *et al.*[9] reasonably well. However, the variation of the rate with the intensity of the infrared seeding light is too rapid to be explained by this model.

We thank Robert M. Pierce for his experimental assistance. Vince Dominic acknowledges fellowship support from the Joint Services Electronics Program.

References

1. U. Österberg and W. Margulis, Opt. Lett. **11**, 516 (1986); Opt. Lett. **12**, 57 (1987).
2. R. H. Stolen and H. W. K. Tom, Opt. Lett. **12**, 585 (1987).
3. A. Kamal, D. A. Weinberger, and W. H. Weber, Opt. Lett. **15**, 613 (1990).
4. V. Mizrahi, Y. Hibino, and G. Stegeman, Opt. Commun. **78**, 283 (1990).
5. A. Kamal, M. L. Stock, A. Szpak, C. H. Thomas, D. A. Weinberger, M. Frankel, J. Nees, K Ozaki, and J. Valdmanis, in *Digest of Optical Society of America Annual Meeting* (Optical society of America, Washington, D. C., 1990), paper PD25.
6. N. M. Lawandy, Opt. Commun. **74**, 180 (1989).
7. N. B. Baranova A. N. Chudinov, and B. Ya. Zel'dovich, Opt. Commun. **79**, 116 (1990).
8. E. M Dianov, P. G. Kazansky, and D. Yu Stepanov, Sov. J. Quantum Electron. **19**, 575 (1989); E. M. Dianov, P. G. Kazansky, and D. Yu Stepanov, Sov. Lightwave Commun. **1**, 247 (1991).
9. D. Z. Anderson, V. Mizrahi, and J. E. Sipe, Opt. Lett. **16**, 796 (1991).
10. The sample was grown by Ensign-Bickford Optical Technologies, Inc. using a hybrid VAD:OVD method. The core was doped to give $\Delta n = 4.5 \times 10^{-3}$.
11. D. M. Krol, M. M. Broer, K. T. Nelson, R. H. Stolen, H. W. K. Tom and W. Pleibel, Opt. Lett. **16**, 211 (1991).
12. I. C. S. Carvalho, W. Margulis, and B. Lesche, Opt. Lett. **16**, 1487 (1991).
13. T. J. Driscoll and N. M. Lawandy, Opt. Lett. **17**, 571 (1992).
14. A. Krotkus and W. Margulis, Appl. Phys. Lett. **52**, 1942 (1988).
15. N. M. Lawandy, Phys. Rev. Lett. **65**, 1745 (1990); M. D. Selker and N. M. Lawandy, Opt. Commun. **81**, 38 (1991).
16. A. Kamal, R. W. Terhune, and D. A. Weinberger, in *International Workshop on Photoinduced Self-Organization Effects in Optical Fiber*, Francois Ouellette, Editor, Proc. SPIE 1516, 137 (1991).

Measuring the coherence length of mode-locked laser pulses in real time

Vince Dominic, X. Steve Yao, R. M. Pierce, and Jack Feinberg
Departments of Physics and Electrical Engineering, University of Southern California, Los Angeles, California 90089-0484

(Received 11 September 1989; accepted for publication 25 November 1989)

We demonstrate a new technique for displaying the electric field autocorrelation function of a laser pulse in real time, using two-beam coupling in a photorefractive crystal. This technique can be used over the entire visible and near-infrared regions of the spectrum, even with weak laser beams, and is automatically self-phase matched.

The coherence length of a laser pulse can be measured by interfering the pulse with its own delayed replica.[1-9] Here we measure the coherence length[10] of a pulse from a mode-locked laser, where we average over many pulses. As suggested by Johnson *et al.*,[11] we make each laser pulse interfere with itself in a photorefractive crystal. However, we improve upon their technique by encoding different time delays across a single laser beam,[12] so that the entire field autocorrelation function can be determined in essentially real time (a few milliseconds). Our technique works over a wide range of wavelengths (limited only by the spectral response of the photorefractive crystal) and with very weak laser pulses (~microwatt average power).

The technique is outlined in Fig. 1. The incident laser beam is split into two, with one beam (the reference beam) directed into a photorefractive crystal. The other beam (the probe beam) illuminates a diffraction grating at grazing incidence. The first-order diffracted beam has different time delays encoded onto its different portions.[12] Inspection of Fig. 1 shows that the left side of the diffracted probe beam travels a shorter distance to the photorefractive crystal than the right side of the diffracted probe beam, and so arrives at the crystal first. This diffracted probe beam is focused by a lens into the photorefractive crystal, where it intersects the reference beam and forms an intensity interference pattern, but only in those regions of the crystal where the two beams are coherent with each other.

The intensity pattern creates an index-of-refraction hologram in the photorefractive crystal. The strength of the hologram depends on the visibility of the intensity interference fringes, which depends on the relative coherence of the two interfering beams. Note that if the incident laser pulses are weak, it may take many pulses to build up the photorefractive hologram. This hologram couples the two beams, so that the probe beam experiences gain (or loss, depending on the orientation of the crystal). A one-dimensional array of detectors measures the profile of the amplified probe beam and stores it in a computer. *The probe beam gain will vary with distance x across the face of the beam, and will depend on the local degree of coherence of the probe beam with the reference beam.* As we show below, the gain profile of the amplified probe beam is simply related to the electric field autocorrelation function of the incident laser beam.

Our coherence length measurement technique can be applied to a train of (almost) arbitrarily weak laser pulses. The photorefractive hologram integrates the intensity interference pattern over time, and reaches a steady-state amplitude that is independent of the total intensity of the incident beams. (However, the time required to reach the steady state will increase if the laser intensity is decreased.) For example, in the experiments reported here, the time-average intensity of the reference beam was 3.3 W/cm^2 (power, 74 mW; beam diameter, 1.7 mm). At this optical intensity, the response time of the crystal was about one-tenth of a second, enabling an essentially "real time" measurement of the coherence length. However, we also tried decreasing the incident laser intensity by a factor of 1000, so that the photorefractive crystal needed a minute or so to build up its hologram, and we still obtained the same value for the average coherence length of each laser pulse.

The device is calibrated as follows. The reference beam is delayed relative to the probe beam by an optical delay line consisting of a retroreflecting prism mounted on a calibrated translation stage. We repeatedly take data with different known time delays, and we measure the translation of the output beam's profile across the reticon array, as shown in Fig. 2. This plot is linear, as expected, and its slope yields the calibration factor of our apparatus.

Here are some experimental details: The photorefractive crystal is a single-domain crystal of $BaTiO_3$, which we use at room temperature without an applied electric field. Both the reference beam and the probe beam are polarized

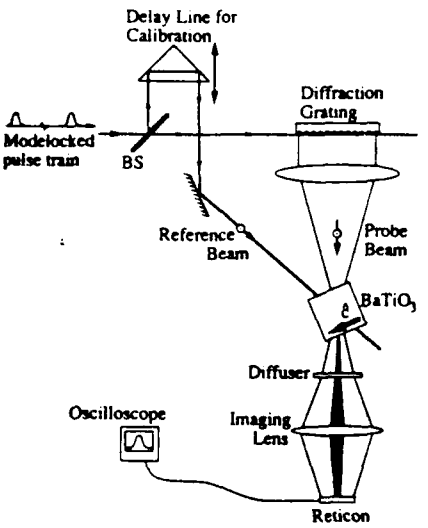

FIG. 1. Optical setup for measuring the average coherence length of a series of optical pulses. The diffraction grating encodes different time delays onto different portions of the probe beam.

 0003-6951/90/060521-03$02.00

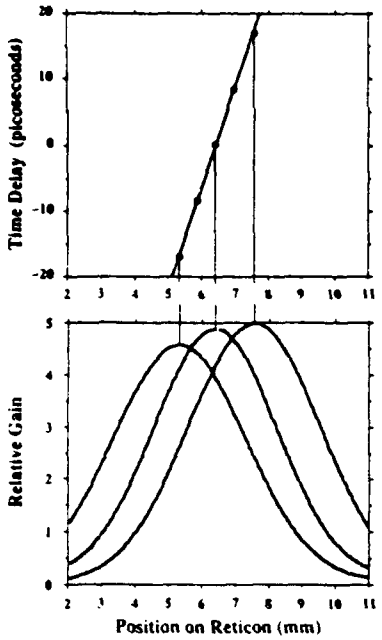

FIG. 2. Calibrating the apparatus. The bottom portion of the figure shows the output beam profile translation across the reticon as the time delay is changed. The top graph shows the linear relationship between the known time delay and the displacement of the beam profile.

perpendicular to the plane of incidence, and both beams are ordinary rays in the $BaTiO_3$ crystal. (Although this choice of polarization has the drawback of reducing the overall two-beam coupling gain of the probe beam, it has the advantage of minimizing two-beam *self*-coupling between the various angular components of the probe beam.) An $f = 25$ cm lens focuses light from the diffraction grating into the $BaTiO_3$ crystal, which is placed one focal length from the lens. The diffraction grating is 5.8 cm square with 1800 lines/mm. The focused probe beam has a full cone angle of 12° outside the crystal. The unfocused reference beam (intensity full width at half maximum = 1.7 mm) and the probe beam are symmetrically incident on the crystal at exterior angles of $\pm$ 19°. The $BaTiO_3$ crystal is oriented with its c axis parallel to the wave vector of the photorefractive hologram, with the crystal's positive c-axis direction chosen to amplify the probe beam. With this geometry the maximum intensity gain of the probe beam is 2–5, depending on which $BaTiO_3$ crystal we use. Depletion of the reference beam was minimized by using a weak probe beam (power = 3 μW). We prevent scattered light from striking the detector array by inserting slits and apertures in both the reference and the probe beams. We reduce speckle noise by inserting a rotating plastic diffuser between the crystal and the detector array, and then imaging the diffuser onto the array. Some of our $BaTiO_3$ crystals have dark storage times of over an hour, so in principle we can integrate laser pulses for that length of time, if desired. However, in practice the useful integration time is limited to no more than a few minutes, due to slow drifts in the position of the mirrors on the optical table.

If the diffraction grating were replaced by a mirror, so that each portion x of the probe beam had the *same* delay τ with respect to the reference beam then the intensity $I_{out}(x)$ of the amplified probe after two-wave mixing in a crystal of length L would be[13]

$$[I_{out}(x) - I_{in}(x)]/I_{in}(x) = |G(\tau)|^2[e^{(\Gamma-\alpha)L} - 1], \quad (1)$$

where $G(\tau)$ is the normalized electric field autocorrelation function of the incident beam, Γ is the intensity two-wave mixing gain per cm for the case of perfectly coherent cw light beams, and α is the intensity absorption coefficient. However, unlike a mirror, the diffraction grating encodes *different* time delays τ on each portion x of the probe beam according to

$$\tau(x) = x(\sin\theta_{in} - \sin\theta_{out})/c\cos\theta_{out}, \quad (2)$$

where x is the transverse distance across the diffracted probe beam, c is the speed of light in air, θ_{in} is the angle between the incident beam and the grating normal, and θ_{out} is the angle between the diffracted beam and the grating normal. At grazing incidence $\theta_{in} = 90°$ and $\theta_{out} = 0°$, so that Eq. (2) simplifies to $\tau(x) = x/c$. The maximum delay τ is limited by the size of the diffraction grating, and was ~190 ps with our 5.8-cm-wide grating.

Equation (1) requires a measurement of the incident probe beam profile $I_{in}(x)$ at the entrance of the crystal. In practice it is simpler to measure the transmitted probe beam after the crystal but in the absence of any two-beam coupling, $I_{\text{no coupling}}(x)$, by blocking the reference beam. Equation (1) becomes

$$\frac{I_{out}(x) - I_{\text{no coupling}}(x)}{I_{\text{no coupling}}(x)} = |G(\tau)|^2[e^{\Gamma L} - e^{\alpha L}] + e^{\alpha L} - 1. \quad (3)$$

This equation includes the effects of Fresnel reflections at the crystal faces, which happen to cancel out nicely. Note that in the absence of linear absorption α, Eq. (3) becomes identical to Eq. (1). For the case of coherent cw illumination, $|G| = 1$, and Eq. (3) reverts to the usual expression describing photorefractive gain.

We tested our device by measuring the average coherence length of the frequency-doubled ($\lambda = 532$ nm) pulses from a mode-locked cw Nd:YAG laser (Coherent Antares 76-s). This laser is actively mode locked and emits pulses at a rate of 76 MHz. Figure 3 shows the relative gain [defined as the left-hand side of Eq. (3)] across the probe beam for a series of ~10^8 laser pulses (i.e., we averaged for ~1 s). The solid line is a least-squares fit of Eq. (3) obtained by varying three parameters: the maximum two-beam coupling gain Γ of the crystal, a vertical offset related to absorption, and the coherence time τ_c of the incident laser pulse. Here we assume that the laser pulses are Gaussian in time, and we take the coherence time τ_c to be the half width at half maximum of the electric field autocorrelation function.[10] From this fit we obtain a value of $\tau_c = 48$ ps. However, we found that τ_c could drift slowly with time by ~8 ps over 30 min, which we attribute to a mode-locking instability of our laser.

In order to test Eq. (3), we tried using two different single-domain crystals of $BaTiO_3$ having dissimilar two-beam coupling gain coefficients Γ. We obtained the same value for the average coherence length of our laser pulses, within experimental error, using either crystal. We also inspected our laser pulses with a 1/4-in.-thick solid glass

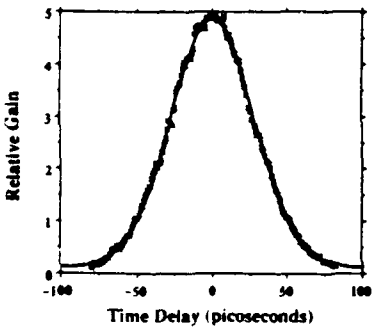

FIG. 3. Plot of the relative intensity gain across the probe beam. Each portion of the beam experiences a different gain because it has been delayed by a different amount of time relative to the reference beam. The horizontal axis shows the relative delay of each portion of the probe beam. The solid line is a best fit to Eq. (3), and yields a coherence time of $\tau_c = 48$ ps.

Fabry–Perot étalon; the appearance of the ring pattern was consistent with the coherence length measured by our two-beam coupling technique. However, the Fabry-Perot also revealed that the center frequency of the laser jittered on the time scale of a few seconds, possibly due to thermally induced fluctuations in the laser's effective cavity length.

What is the resolution limit of this device? Dispersion of the grating will cause spatial broadening of the measured output beam profile $I_{out}(x)$.[12] For the geometry and coherence times used here, this broadening is negligible, but it places a lower limit of 0.1 ps on the shortest pulse we can measure. Also, the finite crossing angle of the two beams will cause a broadening of the output beam profile. The worst case would be for a crossing angle of 90°, which would cause a smearing in time equal to the time it takes light to traverse the wider of the two beams in the crystal. In our experiments, we estimate this smearing to be ~ 1 ps. Our calculations indicate that the effect of a finite recombination time of the photorefractive crystal is to alter the overall two-beam coupling gain coefficient, but without altering the shape of the output profile of the amplified beam.

In summary, we have demonstrated a simple method for measuring the coherence length of a pulsed laser, and especially for a laser that produces a train of very weak optical pulses. This technique does not require phase matching, is simple to align, and can be used over the entire visible and near-infrared regions of the spectrum. The spectral response of our $BaTiO_3$ crystals extends only to the near infrared, and so is too small to be useful at 1.06 μm Nd:YAG laser wavelength. We are pursuing the use of other photorefractive crystals to extend this pulse-measuring technique further into the infrared.

This work was supported by contract No. F49620-88-C-0095 of the Air Force Office of Scientific Research. V. Dominic gratefully acknowledges fellowship support from the National Science Foundation and the Joint Services Electronics Program.

[1] J.-C. M. Diels, E. W. Van Stryland, and D. Gold, In *Picosecond Phenomena*, edited by C. V. Shank, E. P. Ippen, and S. L. Shapiro, Springer Series Chem. Phys. No. 4 (Springer, New York, 1978), pp. 117–120.
[2] R. Trebino, E. K. Gustafson, and A. E. Siegman, J. Opt. Soc. Am. B 3, 1295 (1986).
[3] H. J. Eichler, U. Klein, and D. Langhans, Appl. Phys. 21, 215 (1980).
[4] W. L. Nighan, T. Gong, L. Liou, and P. M. Fauchet, Opt. Commun. 69, 339 (1989).
[5] R. Baltrameyunas, Yu. Vaitkus, R. Danelyus, M. Pyatrauskas, and A. Piskarskas, Sov. J. Quantum Electron. 12, 1252 (1982).
[6] V. S. Idiatulin and Yu. N. Teryaev, Opt. Quantum Electron. 14, 51 (1982).
[7] X. Zhu, K. G. Spears, and J. Serafin, J. Opt. Soc. Am. B 6, 1356 (1989).
[8] J. Janszky, G. Corradi, and D. S. Hamilton, Appl. Opt. 23, 8 (1984).
[9] J. Buchert, R. Dorsinville, P. Delfyett, S. Krimchansky, and R. R. Alfano, Opt. Commun. 52, 433 (1985).
[10] We use the terms "coherence length" and "coherence time" loosely. Our experimental technique measures the field autocorrelation (or fringe visibility) function versus time delay. The width of this function depends on both the pulse duration and the usual coherence time. For more details, see Ref. 7.
[11] A. M. Johnson, A. M. Glass, W. M. Simpson, R. B. Bylsma, and D. H. Olson, in *Annual Meeting OSA Technical Digest* No. 11 (Optical Society of America, Washington, DC, 1988), paper ThC4.
[12] R. Wyatt and E. E. Marinero, Appl. Phys. 25, 297 (1981).
[13] X. S. Yao, V. Dominic, and J. Feinberg (unpublished).

Theory of beam coupling and pulse shaping of mode-locked laser pulses in a photorefractive crystal

X. Steve Yao, Vince Dominic, and Jack Feinberg

Departments of Physics and Electrical Engineering, University of Southern California, Los Angeles, California 90089-0484

Received October 18, 1989; accepted June 28, 1990

We describe how optical beams from a mode-locked laser will couple in a photorefractive crystal. We show that the two-beam-coupling gain coefficient is proportional to the square of the electric field correlation of the incoming light pulses. Consequently we show that two-beam-coupling experiments can measure the average coherence length of mode-locked laser pulses. We also describe how the temporal envelopes of the mode-locked optical pulses distort as they couple and propagate through the photorefractive crystal, and we give examples of how pulses can be shaped by using photorefractive coupling.

1. INTRODUCTION

The strong coupling between optical beams in a photorefractive crystal has been extensively studied for continuous-wave optical beams[1] and for single, short, high-irradiance optical pulses.[2-4] Here we consider the coupling between trains of mode-locked pulses in a photorefractive crystal. We are especially interested in photorefractive crystals that have a long dark-storage time, which permits the light-induced changes caused by successive optical pulses to accumulate in the crystal. We consider the case in which each optical pulse is quite weak, so that it takes a large number of pulses ($>10^6$) to build up a quasi-steady-state refractive-index grating in the crystal. We derive the time-averaged response of the crystal to these pulses. We show that, once formed, the photorefractive grating can alter the temporal shape of the laser pulses as they traverse the crystal. We also show that a photorefractive crystal can be used to measure the average coherenoe length of a train of mode-locked laser pulses, as was recently demonstrated in experiments by Johnson *et al.*[5-7] and Dominic *et al.*[8]

2. SPACE-CHARGE ELECTRIC FIELD

Consider an infinite and periodic train of laser pulses, such as from a cw-pumped mode-locked laser. Let two such pulse trains intersect in a photorefractive crystal. If in some region of the crystal the two beams are coherent (and so produce an intensity-interference pattern there), then charge carriers in the crystal will be rearranged by the pattern of bright and dark fringes. The migration of these charge carriers causes a space-charge field $E_{sc}(\mathbf{r}, t)$ to grow and eventually reach a quasi-equilibrium. Suppose that the energy of each pulse is small, so that many pulses are required in order to reach the steady state. Then, once E_{sc} reaches its quasi-equilibrium value, each subsequent laser pulse causes E_{sc} to make only small excursions that always return it to its initial value, as we show below.

The time dependence of this space-charge field is governned by a first-order differential equation, as derived by Strohkendl *et al.*[9] for the case of constant incident intensity. However, the same equation holds even if the intensity is changing in time, as long as the peak intensity is weak enough to satisfy the restriction of Eq. (8) of Ref. 9. For the case in which the recombination rate of free carriers is much shorter than the pulse duration, the space-charge field evolves according to

$$\frac{\partial E_{sc}(\mathbf{r}, t)}{\partial t} + aI_0(t)E_{sc}(\mathbf{r}, t) = ibE_1(\mathbf{r}, t)E_2^*(\mathbf{r}, t), \qquad (1)$$

where E_{sc} is the magnitude of the (quasi-dc) space-charge field, $E_1(\mathbf{r}, t)$ and $E_2^*(\mathbf{r}, t)$ are the slowly varying complex optical-field envelopes, and $I_0(t) = |E_1(\mathbf{r}, t)|^2 + |E_2(\mathbf{r}, t)|^2$ is proportional to the total intensity. [Note that, in the absence of absorption, energy conservation requires the intensity to be a constant in space, which is why $I_0(t)$ has no spatial dependence.] The quantities a and b are complicated functions of material parameters and beam geometry but not of the optical intensities.[9]

Equation (1) indicates that the space-charge field is driven by the interference term $E_1(\mathbf{r}, t)E_2^*(\mathbf{r}, t)$ and is erased by the uniform intensity I_0. If many pulses are required in order to reach steady state, then no one pulse can change E_{sc} by a large amount, and E_{sc} will reach a quasi-steady-state value that is determined by the balance of the driving and erasing terms. Equation (1) holds when the free-carrier recombination time is much less than the duration of a single mode-locked laser pulse, so that the free-carrier density created by light in the photorefractive material closely follows any variation of the light intensity with time. If this is not the case, the situation becomes more complicated, for we must then couple Eq. (1) to another differential equation that describes the time evolution of the free-carrier density. We discuss this case at the end of this section.

Because in general the incoming laser pulses are not identical, we must average over the ensemble of possible

0740-3224/90/122347-09$02.00

pulses. The laser pulses may fluctuate both in amplitude and in phase. We choose to model the pulses as having identical amplitudes but randomly varying phases. To our knowledge there is no satisfactory statistical description of phase fluctuations of mode-locked laser pulses, so we will not specify the statistics of the phase fluctuations; instead, we simply characterize the optical electric field of the pulses by a parameter τ_s, which specifies the characteristic length of time (averaged over many pulses) during which the optical electric fields evolve sinusoidally in time without interruption. (An analogy may be an electron drifting freely through a solid, with some average time between collisions.)

Using our amplitude-stabilized pulses, we take the ensemble average of Eq. (1):

$$\frac{\partial \overline{E_{sc}(\mathbf{r},t)}}{\partial t} + aI_0(t)\overline{E_{sc}(\mathbf{r},t)} = ib\overline{E_1(\mathbf{r},t)E_2^*(\mathbf{r},t)}, \tag{2}$$

where the overbar denotes an ensemble average.[10] For the case of cw illumination, Eq. (2) can be solved by a steady-state space-charge field E_{sc} that is proportional to the modulation of the intensity interference pattern.[11] For the case of pulsed illumination, we expect the equilibrium value of the space-charge field to depend in a similar manner also on the modulation of the optical intensity and therefore on the relative coherence of the two optical pulses at the crystal. We postulate that the steady-state solution of Eq. (2) is

$$\overline{E_{sc}} = \frac{ib}{a}\frac{\langle \overline{E_1(\mathbf{r},t)E_2^*(\mathbf{r},t)}\rangle}{\langle |E_1(\mathbf{r},t)|^2 + |E_2(\mathbf{r},t)|^2\rangle}, \tag{3}$$

where the the notation $\langle\ \rangle$ denotes an average over time T:

$$\langle F(t)\rangle = \frac{1}{T}\int_{-T/2}^{T/2} F(\tau)\,d\tau. \tag{4a}$$

Note that, if the interfering beams are cw, then the time averages in Eq. (3) may be dropped, and we obtain the usual dependence of the steady-state space-charge field on the modulation of the intensity-interface pattern.[11] For periodic optical pulses, the postulated dependence of Eq. (3) may be viewed as the dc term in a temporal Fourier expansion of E_{sc}. We show below that this dc term is by far the largest term (by a factor of 10^6) in the expansion, again because many pulses are required in order to reach the quasi-equilibrium, so that no one pulse can push E_{sc} far from its equilibrium value.

Using the notation of Trebino *et al.*[12] we can express the electric-field envelope of the optical pulses as

$$E_1(\mathbf{r},t) = A_1(\mathbf{r},t)u_1(\mathbf{r},t), \tag{4b}$$

$$E_2(\mathbf{r},t) = A_2(\mathbf{r},t-\tau_d)u_2(\mathbf{r},t-\tau_d), \tag{4c}$$

where in Eqs. (4) the functions $A_1(\mathbf{r},t)$ and $A_2(\mathbf{r},t)$ are the deterministic amplitude of the pulses of beams 1 and 2, respectively. The functions $u_1(\mathbf{r},t)$ and $u_2(\mathbf{r},t)$ are statistical factors that contain information about the phase fluctuations of the two beams; both of these functions are normalized to unity: $|u_1| = |u_2| = 1$. For convenience we have defined beam 2 with a built-in delay time τ_d, because in practice the two interfering optical beams are usually derived by splitting one single beam into two and then delaying one beam with respect to the other by a time τ_d. Using this notation, we may rewrite the numerator of Eq. (3) as

$$G(\tau_d) \equiv \langle \overline{E_1(\mathbf{r},t)E_2^*(\mathbf{r},t)}\rangle = \langle A_1(\mathbf{r},t)A_2^*(\mathbf{r},t-\tau_d)\overline{u_1(\mathbf{r},t)u_2^*(\mathbf{r},t-\tau_d)}\rangle. \tag{5}$$

When the phase fluctuations are governed by jointly wide-sense stationary statistics,[13] so that the quantity $\overline{u_1(\mathbf{r},t)u_2^*(\mathbf{r},t-\tau_d)}$ is independent of time,[14] we express Eq. (5) as

$$G(\tau_d) = \langle A_1(\mathbf{r},t)A_2^*(\mathbf{r},t-\tau_d)\rangle\gamma^{(2)}(\tau_d), \tag{6}$$

where $\gamma^{(2)}(\tau_d)$ is the second-order coherence function, which depends on the relative delay τ_d between the two pulses (and implicitly on the parameter τ_s, the average phase-coherence time of a pulse):

$$\gamma^{(2)}(\tau_d) \equiv \overline{u_1(\mathbf{r},t)u_2^*(\mathbf{r},t-\tau_d)}. \tag{7}$$

Substituting Eq. (7) into Eq. (3) yields

$$\overline{E_{sc}} = \frac{ib}{a}\frac{\langle A_1(\mathbf{r},t)A_2^*(\mathbf{r},t-\tau_d)\rangle\gamma^{(2)}(\tau_d)}{I_0}. \tag{8}$$

In order to verify our guess that Eq. (8) is indeed the quasi-steady-state solution for the space-charge field, we numerically integrated Eq. (1) for the case of a periodic train of pulses, with the amplitude of each pulse taken to be Gaussian in time. At first we assumed that each pulse was transform limited. Using a fourth-order Runge–Kutta method, we computed how E_{sc} changed during each light pulse. Figures 1 and 2 show the deviation of E_{sc} from the steady-state value predicted by Eq. (8). In Fig. 1(a) we set the relative delay between the two writing beams (one strong and the other weak) to be $\tau_d = -30$ psec (so that the strong beam arrives before the weak beam). In Fig. 1(b) the space-charge field is seen first to decay and then to grow during each laser pulse but always to return to its initial value. Figure 2 shows the result for $\tau_d = +70$ psec (where now the strong beam arrives after the weak beam). Here each laser pulse causes the space-charge field first to decay (slightly) when the weak beam arrives, then to grow, and then to decay back to its steady-state value. Note that the vertical scale in Figs. 1(b) and 2(b) is in parts in 10^6; the maximum excursion of the space-charge field from its steady-state value (which it maintains between laser pulses) is quite small. When we picked a value for E_{sc} that was too small, we found that after the next light pulse E_{sc} would be left at a slightly larger value than when it started, until after many light pulses it attained the steady-state value specified by Eq. (8). Similarly, when we initially picked E_{sc} too large, then the next light pulse would leave it slightly smaller. Only with the value of E_{sc} given by Eq. (8) would each light pulse cause the space-charge field to return to exactly the same value that it had before the light pulse.

To generate Figs. 1 and 2, we used material parameters that are typical for photorefractive $BaTiO_3$ and optical beams with average beam intensities of tens of milliwatts per square millimeter and pulse durations of 70 psec (intensity FWHM). For this calculation we assumed that (a) the dark decay rate is much less than the pulse repeti-

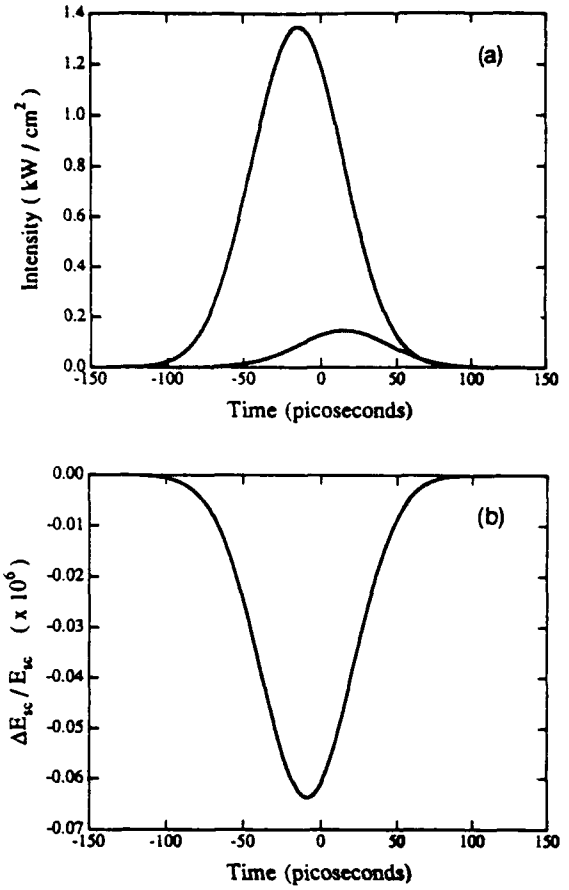

Fig. 1. (a) A strong optical beam leads a weak beam by 30 psec. (b) While these optical pulses are present in the crystal, the space-charge field momentarily deviates from its steady-state value: It initially decays and then recovers.

tion rate, (b) the average modulation of the photorefractive grating is much less than unity, (c) there are no shallow traps, (d) there is no spatially uniform dc electric field in the crystal, (e) the spatially periodic free-carrier number density is much less than the spatially periodic deep-trap number density,[9] (f) and the recombination time of charges in the band is much less than the duration of each laser pulse.

We also considered the case in which the optical pulses have phases that vary randomly in time, and we found that the quasi-steady-state space-charge field is still given by the correlation of the two optical fields, as predicted by Eq. (8). Encouraged by these results, we then tried relaxing condition (f) above by making the recombination time longer than the pulse duration by factors ranging from 1 to 140 (while keeping constant the product of mobility and recombination time). We found that the space-charge field still attained the value given by Eq. (8) to within 1 part in 10^7.

3. COUPLED-WAVE EQUATIONS

As discussed in Section 2, the interference of two weak, infinite trains of optical pulses eventually produces a quasi-steady-state space-charge field in a photorefractive crystal. This electric field alters the refractive index of the crystal; it creates a refractive-index grating. Here we discuss how the optical beams are coupled by this grating. In particular, as the beams traverse the crystal their temporal shapes are modified by their coupling with the grating, which then alters the grating, which then alters the beams, which makes the equations difficult to solve. Coupled-wave treatments[1] of this problem usually ignore any variation in the temporal envelopes of the pulses as they propagate through the crystal. Here we include these variations.

To derive the coupled-wave equations, we consider a material with no free currents. Maxwell's equations then yield

$$\nabla^2 \mathcal{E}(\mathbf{r},t) - \mu_0 \frac{\partial^2 \mathcal{D}(\mathbf{r},t)}{\partial t^2} = 0, \tag{9}$$

where $\mathcal{E}(\mathbf{r},t)$ is the total real optical electric field in the material and $\mathcal{D}(\mathbf{r},t)$ is the corresponding real displacement vector. In Eq. (9) we ignore the term $\nabla(\nabla \cdot \mathcal{E})$.[15]

Now let the total optical field comprise two light beams with the same nominal frequency ω_0, respective complex electric fields E_1 and E_2, wave vectors $\mathbf{k}_1$ and $\mathbf{k}_2$, and eigenpolarizations $\hat{e}_1$ and $\hat{e}_2$ in the crystal. The total optical electric field and displacement vectors are

$$\begin{aligned}\mathcal{E}(\mathbf{r},t) = \mathrm{Re}\{[&\hat{e}_1 E_1(\mathbf{r},t)\exp(i\mathbf{k}_1 \cdot \mathbf{r}) \\ &+ \hat{e}_2 E_2(\mathbf{r},t)\exp(i\mathbf{k}_2 \cdot \mathbf{r})]\exp(-i\omega_0 t)\},\end{aligned} \tag{10}$$

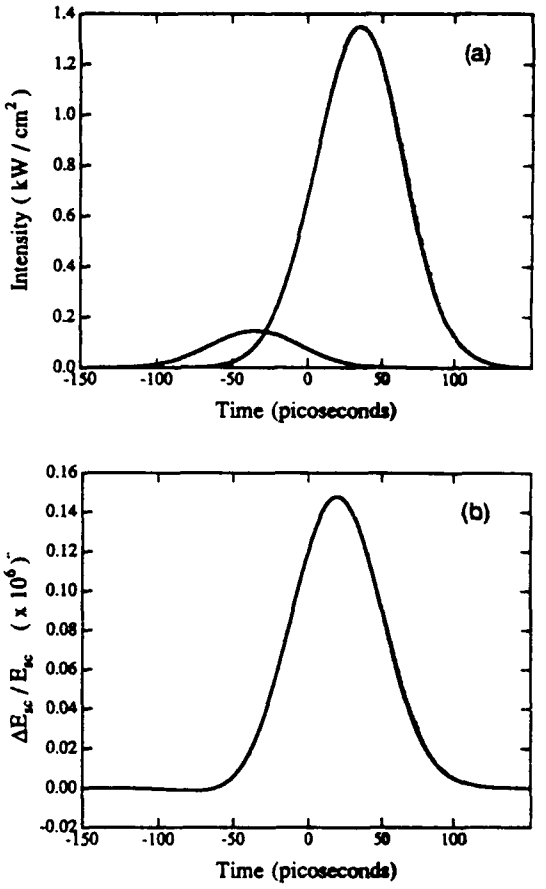

Fig. 2. (a) A strong optical beam follows a weak beam by 70 psec. (b) While these pulses are present, the space-charge field grows and then decays, but it never deviates by even 1 part in 10^6 from its steady-state value.

$$\mathcal{D}(\mathbf{r},t) = \mathrm{Re}\{[\mathbf{D}_1(\mathbf{r},t)\exp(i\mathbf{k}_1\cdot\mathbf{r}) + \mathbf{D}_2(\mathbf{r},t)\exp(i\mathbf{k}_2\cdot\mathbf{r})]\exp(-i\omega_0 t)\}, \quad (11)$$

$$\mathbf{D}_i(\mathbf{r},t) \equiv \varepsilon_0\bar{\varepsilon}(\mathbf{r})\cdot\hat{e}_i E_i(\mathbf{r},t), \qquad i = 1,2. \quad (12)$$

In Eqs. (10)–(12), ε_0 is the permittivity of free space, $\bar{\varepsilon}_r(\mathbf{r})$ is the relative dielectric tensor of the medium, and $\mathbf{D}_i(\mathbf{r},t)$ and $\hat{e}_i E_i(\mathbf{r},t)$ are the slowly varying envelopes of the displacement and the electric-field vectors at the optical frequency ω_0. Note that Eq. (12) ignores any material dispersion. For laser pulses that are picoseconds or longer, this approximation is justified by the short length of typical photorefractive crystals. For example, a 2-mm sample of barium titanate would require a pulse duration of less than 100 fsec before group-velocity dispersion would become noticeable.

The interference pattern of the two light beams will have a periodicity $\cos(\mathbf{k}_g\cdot\mathbf{r})$, where $\mathbf{k}_g \equiv \mathbf{k}_1 - \mathbf{k}_2$. The dielectric tensor of the crystal will be altered by the light pattern at the same spatial frequency $\mathbf{k}_g$:

$$\bar{\varepsilon}(\mathbf{r}) = \bar{\varepsilon}_r + \mathrm{Re}[\Delta\bar{\varepsilon}_r\cdot\exp(i\mathbf{k}_g\cdot\mathbf{r})], \quad (13)$$

where $\bar{\varepsilon}_r$ is the crystal's average dielectric tensor. The spatially periodic part of the dielectric tensor $\mathrm{Re}[\Delta\bar{\varepsilon}_r\cdot\exp(i\mathbf{k}_g\cdot\mathbf{r})]$ will couple the two optical waves. Substituting Eqs. (10)–(13) into Eq. (9) yields equations that couple the slowly varying electric-field envelopes E_1 and E_2 of the two optical beams:

$$\left(\frac{\partial}{\partial z} + \frac{1}{v}\frac{\partial}{\partial t}\right)E_1(z,t) = \frac{i\omega}{4n_1 c\cos\theta}(\hat{e}_1^*\cdot\Delta\bar{\varepsilon}_r\cdot\hat{e}_2)E_2(z,t), \quad (14a)$$

$$\left(\frac{\partial}{\partial z} + \frac{1}{v}\frac{\partial}{\partial t}\right)E_2(z,t) = \frac{i\omega}{4n_2 c\cos\theta}(\hat{e}_2^*\cdot\Delta\bar{\varepsilon}_r^*\cdot\hat{e}_1)E_1(z,t). \quad (14b)$$

In Eqs. (14), z is the distance along the bisector of $\mathbf{k}_1$ and $\mathbf{k}_2$ in the crystal, θ is the half-angle between $\mathbf{k}_1$ and $\mathbf{k}_2$, and v is defined as

$$v \equiv (c/n)\cos\theta. \quad (15)$$

For cw beams the time derivatives in the coupled-wave equations (14) are zero, but for pulsed laser beams these time derivatives must be included. Smirl *et al.*[2] included these time derivatives in their analysis of beam coupling in photorefractive crystals with single-shot, high-irradiance laser pulses. However, they did not discuss the evolution of the laser pulses' temporal shapes, and with good reason: in the case that they considered, the energy coupling between the two beams was so small that its effect on the temporal shape of the laser pulses could safely be neglected. Here the energy coupling between the beams can be quite strong, and it can drastically alter the temporal shapes of the light pulses. We discuss such pulse shaping in Section 6.

In deriving the coupled-wave equations (14), we made the following assumptions: The optical electric-field envelope changes slowly with distance:

$$\left|\frac{\partial^2 E_i}{\partial z^2}\right| \ll k_i\left|\frac{\partial E_i}{\partial z}\right|, \quad (16)$$

and with time:

$$\left|\frac{\partial^2(\bar{\varepsilon}\cdot\hat{e}_i E_i)}{\partial t^2}\right| \ll \omega\left|\frac{\partial(\bar{\varepsilon}\cdot\hat{e}_i E_i)}{\partial t}\right|, \quad (17a)$$

$$\left|\frac{\partial(\Delta\bar{\varepsilon}_r\cdot\hat{e}_i E_i)}{\partial t}\right| \ll \omega|\Delta\bar{\varepsilon}_r\cdot\hat{e}_i E_i|. \quad (17b)$$

We assume that the perturbation of the dielectric tensor is small:

$$\Delta\bar{\varepsilon}_r \ll \bar{\varepsilon}_r, \quad (18)$$

and that all the frequency components of the laser pulses are perfectly Bragg matched to the grating. We also assume that these frequency components all write the same grating. (For a millimeter-sized grating, this implies a minimum laser pulse width of a few tens of picoseconds.)

4. PHOTOREFRACTIVE GRATING

The space-charge field E_{sc} of Eq. (8) will induce a change in the dielectric tensor by the electro-optic (Pockels) effect[11]:

$$\Delta\bar{\varepsilon}_r = -\bar{\varepsilon}_r\cdot(\bar{\mathbf{R}}\cdot\hat{k}_g)\cdot\bar{\varepsilon}_r\overline{E_{sc}}, \quad (19)$$

where $\bar{\mathbf{R}}$ is the electro-optic tensor of the crystal. Equation (19) ignores any contribution of $\Delta\bar{\varepsilon}_r$ from electrons in the conduction band, i.e., the free-electron grating.[2–4] Because this transient grating disappears in the time between each laser pulse, at the intensities used in our calculations the free-carrier grating will be negligible compared with the steady-state photorefractive grating, which accumulates over many laser pulses. For example, even with a pulse energy as large as 6 mJ/cm^2, the peak diffraction efficiency of just the transient free-carrier grating in $BaTiO_3$ is only 10^{-4},[3] which is 200 times smaller than the steady-state diffraction efficiency with cw beams in the same geometry. Because the diffraction efficiency from a free-carrier grating depends quadratically on the fluence of the writing pulses,[3] with a cw mode-locked laser having a fluence of microjoules per square centimeter, the diffraction efficiency from the free-carrier grating will be on the order of 10^{-9}, which can certainly be ignored. Note that any contribution to $\bar{\varepsilon}_r$ from an absorption grating[16–19] can be included in our coupled-wave equations by changing the overall two-beam-coupling gain coefficient.

Substituting Eqs. (8) and (19) into the coupled-wave equations (14) yields

$$\left(\frac{\partial}{\partial z} + \frac{1}{v}\frac{\partial}{\partial t}\right)E_1(z,t) = \eta_{12}\frac{G(z,\tau_d)}{I_0}E_2(z,t), \quad (20a)$$

$$\left(\frac{\partial}{\partial z} + \frac{1}{v}\frac{\partial}{\partial t}\right)E_2(z,t) = -\eta_{21}^*\frac{G^*(z,\tau_d)}{I_0}E_1(z,t), \quad (20b)$$

where, with plane waves incident upon the crystal, the field correlation function G defined in Eq. (5) is now permitted to vary only along the z direction. In Eqs. (20a) and (20b) the coupling constants η_{ij} are

$$\eta_{12} = \frac{\omega}{4n_1 c\cos\theta}\frac{b}{a}[\hat{e}_1^*\cdot\bar{\varepsilon}_r\cdot(\bar{\mathbf{R}}\cdot\hat{k}_g)\cdot\bar{\varepsilon}_r\cdot\hat{e}_2], \quad (21a)$$

$$\eta_{21}^* = \frac{\omega}{4n_2c\cos\theta}\frac{b^*}{a^*}[\hat{e}_2^* \cdot (\bar{\varepsilon}_r \cdot (\bar{\mathbf{R}} \cdot \hat{k}_g) \cdot \bar{\varepsilon}_r)^* \cdot \hat{e}_1]. \quad (21b)$$

We combine Eqs. (20), perform an ensemble average over many pulses, and average over the time T between optical pulses:

$$\frac{\partial\langle|\overline{E_1(z,t)}|^2\rangle}{\partial z} = +2\,\mathrm{Re}(\eta_{12})\frac{|G(z,\tau_d)|^2}{I_0}, \quad (22a)$$

$$\frac{\partial\langle|\overline{E_2(z,t)}|^2\rangle}{\partial z} = -2\,\mathrm{Re}(\eta_{21})\frac{|G(z,\tau_d)|^2}{I_0}, \quad (22b)$$

$$\frac{\partial G(z,\tau_d)}{\partial z} = \frac{G(z,\tau_d)}{I_0}(\eta_{12}\langle|\overline{E_2}|^2\rangle - \eta_{21}\langle|\overline{E_1}|^2\rangle). \quad (22c)$$

In deriving Eqs. (22) we eliminate the time derivatives by using the fact that

$$\left\langle \frac{\partial}{\partial t}F(z,t)\right\rangle = 0 \quad (23)$$

for any function F that has a period T.

If the time-averaged intensity of beam 1 is much less than that of beam 2, ($\langle|\overline{E_1}|^2\rangle \ll \langle|\overline{E_2}|^2\rangle$), then the intensity of the strong beam remains constant over the interaction length ($\langle|\overline{E_2}|^2\rangle \cong I_0$), and the above equations have the simple solutions:

$$G(z,\tau_d) = G(0,\tau_d)\exp(\eta_{12}z), \quad (24)$$

$$\langle|\overline{E_1(z,t)}|^2\rangle - \langle|\overline{E_1(0,t)}|^2\rangle = \frac{|G(0,\tau_d)|^2\exp[(g_{12}z) - 1]}{I_0}, \quad (25)$$

where the gain coefficient g_{12} is defined as

$$g_{12} \equiv 2\,\mathrm{Re}(\eta_{12}). \quad (26)$$

Equation (25) states that the average intensity gain of the weak beam is proportional to the magnitude squared of the correlation function of the two incident beams. One factor of the correlation function appears because the two beams must first interfere to create the refractive-index grating; the second factor appears because each beam, after diffraction off the grating, interferes with the transmitted fraction of the other beam. Our result is an interesting contrast to that of Trebino *et al.*,[12] who analyzed the interaction of two beams in a rapidly responding absorptive medium.[20–24] In that case the grating was newly formed by each laser pulse and decayed to zero between pulses. Consequently the average intensity of their diffracted beam was proportional to the fourth-order coherence function of the two interacting beams. In contrast, in our case the grating in the photorefractive crystal is formed by a large number of pulses and reaches a steady state. The early pulses create the grating; the later pulses diffract off the grating. Consequently, the intensity of the transmitted beam is proportional to the product of two second-order coherence functions and not to the fourth-order coherence function.

Equation (25) also shows that the average intensity of the weak beam grows at a rate determined by the electric-field correlation function $G(0,\tau_d)$ evaluated at the entrance face of the crystal, even though the temporal profiles of the two beams can change dramatically during propagation, as we show below. It is convenient to separate the incident, deterministic optical-field envelopes $A_i(0,t)$ into a real amplitude E_{i0} and a normalized complex temporal profile $\mathcal{T}_i(t)$ [so that the peak value of $\mathcal{T}_i(t)$ is unity]:

$$A_i(0,t) = E_{i0}\mathcal{T}_i(t), \qquad i = 1,2. \quad (27)$$

This permits us to define the normalized field correlation function $\Gamma(\tau_d)$:

$$\Gamma(\tau_d) \equiv \frac{\langle\mathcal{T}_1(t)\mathcal{T}_2^*(t-\tau_d)\rangle}{[\langle|\mathcal{T}_1(t)|^2\rangle\langle|\mathcal{T}_2(t)|^2\rangle]^{1/2}}\gamma^{(2)}(\tau_d). \quad (28)$$

Then substitution into Eq. (25) yields

$$\frac{\langle|\overline{E_1(z,t)}|^2\rangle - \langle|\overline{E_1(0,t)}|^2\rangle}{\langle|\overline{E_1(0,t)}|^2\rangle} = [\exp(g_{12}z) - 1]|\Gamma(\tau_d)|^2. \quad (29)$$

Equation (29) is the central result of our theory; it shows that after the weak beam has traversed a distance z in the crystal, its intensity gain depends on the magnitude squared of the normalized electric-field correlation function $\Gamma(\tau_d)$. For a given time delay τ_d, the function $\Gamma(\tau_d)$ is a measure of the fringe visibility of the interfering optical beams. Note that, for the case of cw light beams having infinite coherence time, $|\Gamma(\tau_d)|$ becomes unity, and the intensity of the weak wave grows exponentially with distance, as expected[1]:

$$\langle|\overline{E_1(z,t)}|^2\rangle = \langle|\overline{E_1(0,t)}|^2\rangle\exp(g_{12}z). \quad (30)$$

5. MEASURING COHERENCE OF LIGHT PULSE

Now we show how a slow photorefractive crystal can be used to measure the autocorrelation of a fast laser pulse, as experimentally demonstrated by Johnson *et al.*[5–7] and by Dominic *et al.*[8]

Let the incident laser beam be split into two beams and recombined in a photorefractive crystal, with a relative time delay τ_d between the two beams. Measure the coupling gain [defined by Eq. (29)] as a functon of τ_d. According to Eq. (29), the resulting plot will be proportional to the square of the electric-field autocorrelation of the incoming laser pulses.

As an example, consider transform-limited laser pulses whose intensity profiles are Gaussian in time with a FWHM of τ_p. A plot of the measured intensity-coupling gain versus τ_d for these pulses will be a Gaussian curve with a FWHM of $2\tau_p$.

One can also consider the case of a cw beam with a limited coherence length, for example, a beam with a Gaussian power spectrum (and therefore a Gaussian coherence function, from the Wiener–Khinchin theorem):

$$\gamma^{(2)}(\tau_d) = \exp[-(\tau_d^2/\tau_s^2)\ln 2], \quad (31)$$

where τ_s is the average phase coherence time. In that case the plot of beam-coupling gain versus τ_d will trace out a Gaussian with a FWHM of $2\tau_s$.

Finally, we consider the more general case in which the light is pulsed and not transform limited. The electric-field envelope of the optical wave is

$$E(0,t) = E_0 \exp[i\varphi(t)]\exp[-2(t^2/\tau_p^2)\ln 2], \quad (32)$$

where the phase $\varphi(t)$ of the wave may be varying randomly with time. For this pulse Eq. (28) gives a coherence function $\Gamma(\tau_d)$:

$$\Gamma(\tau_d) = \exp\left[-\tau_d^2\left(\frac{1}{\tau_p^2} + \frac{1}{\tau_s^2}\right)\ln 2\right], \quad (33)$$

where, in analogy with the cw case, we assume that the phase correlation is also Gaussian, so that the ensemble average of the correlation of the phase functions [as described in Eq. (7)] is

$$\gamma^{(2)}(\tau_d) = \exp[-(\tau_d^2/\tau_s^2)\ln 2], \quad (34)$$

where τ_s is the average phase coherence time. For this case of non-transform-limited pulses the measured gain will be a Gaussian function of the relative time delay τ_d with a FWHM[25] of

$$\text{FWHM} = \frac{2\tau_p\tau_s}{(\tau_p^2 + \tau_s^2)^{1/2}}. \quad (35)$$

6. PULSE SHAPING

The photorefractive grating not only alters the intensity of each beam but also alters the temporal shape of the pulses as they traverse the crystal. These pulse-shape changes are not limited by the response time of the crystal.

Consider the case in which two optical beams have already built up a steady-state grating in the crystal. Each beam diffracts off this grating and interferes with the other beam, which drastically alters the temporal pulse shapes of both beams, as shown in Fig. 3.

To describe pulse shaping by photorefractive two-beam coupling quantitatively, we use a Fourier representation of the optical-pulse envelopes E_1 and E_2:

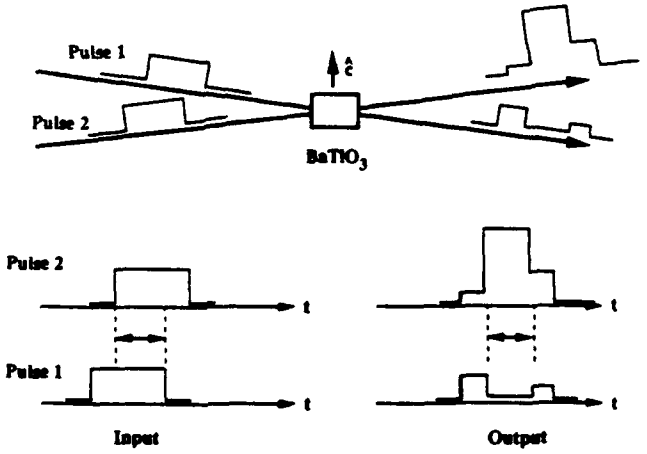

Fig. 3. Schematic illustrating pulse shaping by two-beam coupling in a photorefractive crystal. The square temporal profiles of the two incident pulses are altered after coupling in the crystal. [A steady-state grating has already been built up in the crystal, and each new light pulse barely perturbs this grating (see Figs. 1 and 2)]. Note that when the two pulses overlap in time the transmitted field of pulse 2 constructively interferes with the diffracted field of pulse 1, while the transmitted field of pulse 1 destructively interferes with the diffracted field of pulse 2. When the two pulses do not overlap, there is no interference.

$$E_{1,2}(z,t) = \frac{1}{2\pi}\int_{-\infty}^{\infty} E_{1,2}(z,\omega)e^{-i\omega t}\,d\omega. \quad (36)$$

In the frequency domain the coupled-wave equations (20) become

$$\frac{\partial F_1(z,\omega)}{\partial z} = +\eta_{12}\frac{G(z,\tau_d)}{I_0}F_2(z,\omega), \quad (37a)$$

$$\frac{\partial F_2(z,\omega)}{\partial z} = -\eta_{21}^*\frac{G^*(z,\tau_d)}{I_0}F_1(z,\omega), \quad (37b)$$

where for convenience we have defined

$$F_1(z,\omega) \equiv \exp\left(-\frac{i\omega z}{v}\right)E_1(z,\omega), \quad (38a)$$

$$F_2(z,\omega) \equiv \exp\left(-\frac{i\omega z}{v}\right)E_2(z,\omega). \quad (38b)$$

Equations (37a) and (37b) are solved using Eq. (24) and the boundary conditions

$$F_1(0,\omega) = E_1^0, \quad (39a)$$

$$F_2(0,\omega) = E_2^0, \quad (39b)$$

$$\left.\frac{\partial F_1(z,\omega)}{\partial z}\right|_{z=0} = +\eta_{12}\frac{G(0,\tau_d)}{I_0}E_2^0, \quad (39c)$$

$$\left.\frac{\partial F_2(z,\omega)}{\partial z}\right|_{z=0} = -\eta_{21}^*\frac{G^*(0,\tau_d)}{I_0}E_1^0 \quad (39d)$$

and then transforming the solutions $F_1(z,\omega)$ and $F_2(z,\omega)$ back into the time domain. The resulting solution for the electric-field envelope of each pulse as it propagates a distance z through the crystal is then

$$E_1(z,t) = E_1\left(0, t - \frac{z}{v}\right)\cos|\beta(z,\tau_d)| + \frac{\Gamma(\tau_d)}{|\Gamma(\tau_d)|}E_2\left(0, t - \frac{z}{v}\right)\sin|\beta(z,\tau_d)|, \quad (40a)$$

$$E_2(z,t) = E_2\left(0, t - \frac{z}{v}\right)\cos|\beta(z,\tau_d)| - \frac{\Gamma^*(\tau_d)}{|\Gamma(\tau_d)|}E_1\left(0, t - \frac{z}{v}\right)\sin|\beta(z,\tau_d)|, \quad (40b)$$

where the function $\beta(z,\tau_d)$ is defined as

$$\beta(z,\tau_d) \equiv \frac{G(0,\tau_d)}{I_0}(e^{\eta z} - 1) = \left[\frac{\langle|E_1(0,t)|^2\rangle}{\langle|E_2(0,t)|^2\rangle}\right]^{1/2}\Gamma(\tau_d)(e^{\eta z} - 1). \quad (41)$$

In Eqs. (40) we have assumed that the time-averaged intensity of beam 1 is much less than that of beam 2: i.e., $\langle|E_1|^2\rangle \ll \langle|E_2|^2\rangle$. For simplicity we have also assumed that both of the coupling constants η_{12} and η_{21} are real and equal, so that $\eta = \eta_{12} = \eta_{21}^*$. $\Gamma(\tau_d)$ is the normalized field correlation of beams 1 and 2, as defined in Eq. (28). Beam 1 will either gain or lose energy during its propagation through the crystal according to whether the sign of η is positive or negative.

Equations (40) show that $E_1(z,t)$ is a weighted sum of the input fields $E_1[0, t - (z/v)]$ and $E_2[(0, t - (z/v)]$ at the entrance face of the crystal, with a similar expression for beam 2. The relative weights in the sum depend on the correlation between the two input fields, their relative time delay, and the ratio of their average intensity. To confirm Eqs. (40) we used Eq. (40a) to calculate the time-averaged intensity of the weak beam at an arbitrary position z, and we obtained the same result as with Eq. (25).

As an example of how two-beam coupling can dramatically alter the shape of an optical pulse, consider a train of short pulses (E_2) and a train of somewhat longer pulses (E_1) incident upon the crystal. The short and the long pulses are assumed to have the same spectral width. Assume that the short pulse is transform limited and Gaussian in time and that the long pulse is also Gaussian in time but is chirped. Let these two pulse trains interfere in a photorefractive crystal. Orient the c axis of the crystal so that the longer pulse loses energy as it propagates through the crystal (i.e., make the coupling constant

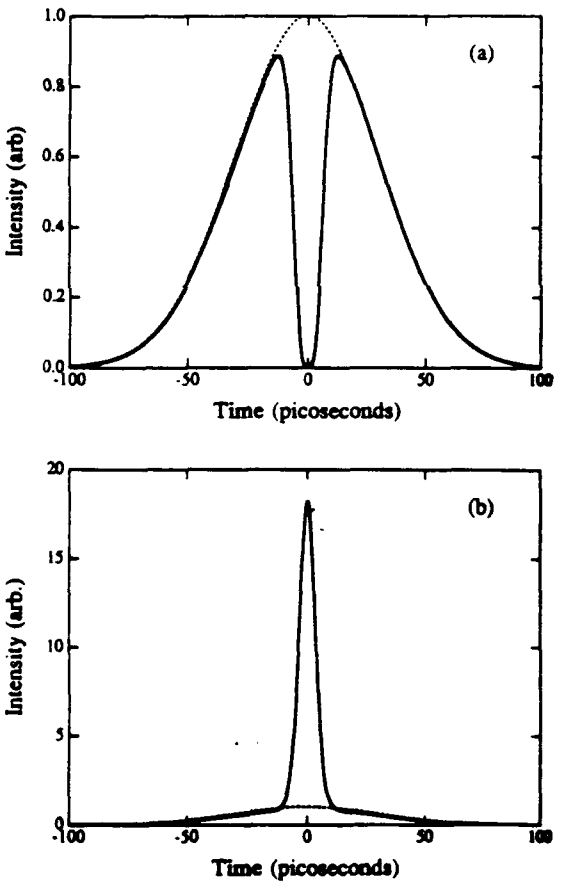

Fig. 4. Pulse shaping by using Gaussian pulses with the same spectral width. The peaks of both beams reach the entrance face of the crystal at the same time ($\tau_d = 0$), but the duration of beam 1 is 10 times greater than that of beam 2. (a) The temporal profile of beam 1 before (dotted curve) and after (solid curve) the photorefractive crystal. Note that beam 2 couples energy out of beam 1. We assume an incident average intensity ratio of $I_2/I_1 = 100$ and a coupling strength $\eta L = -1.23$. (b) The temporal profile of beam 1 before (dotted curve) and after (solid curve) coupling in the crystal. Here we reverse the direction of energy coupling in the crystal, so that beam 2 couples energy into beam 1. We use an incident average intensity ratio of $I_2/I_1 = 100$ and a couping strength $\eta L = +1.23$.

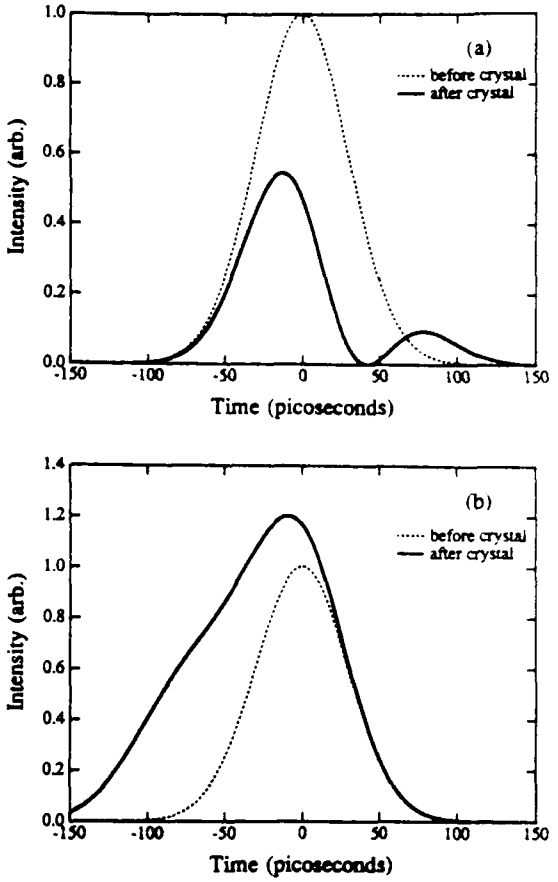

Fig. 5. Pulse shaping in a photorefractive crystal by using equal-width, transform-limited Gaussian pulses (FWHM intensity = 70 psec). The curves show the temporal envelope of incident beam 1 before the crystal (dotted curves) and after the crystal (solid curves). (a) Beam 1 arrives 50 psec before beam 2. The coupling strength is set at $\eta L = -2$ (so that beam 1 loses energy), and the average intensity ratio is set at $I_2/I_1 = 10$. (b) Beam 1 arrives 85 psec before beam 2. The coupling strength is set at $\eta L = +1.5$ (so that beam 1 gains energy), and the average intensity ratio is set at $I_2/I_1 = 100$.

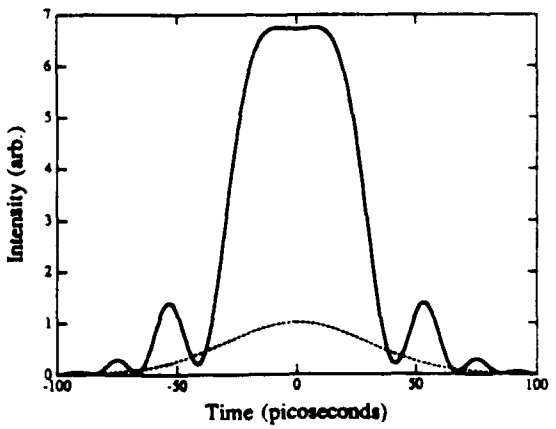

Fig. 6. Pulse shaping in a photorefractive crystal by using Gaussian pulses with the same temporal width (FWHM intensity 70 psec). The temporal envelope of the incident beam (1) is shown before the crystal (dotted curve) and after the crystal (solid curve). Here beam 1 is transform limited, but beam 2 is chirped and has a spectral width 8 times that of beam 1. The time delay between the two beams is zero, and the coupling strength is $\eta L = 1.5$ (beam 1 gains energy).

$\eta < 0$). For these conditions Fig. 4(a) shows that the long pulse will have a deep hole carved out of its center: a dark pulse. Such a pulse may prove useful for the experiments with dark pulses.[26,27] (See Appendix A for further discussion of this calculation.)

If we reorient the crystal so that the longer pulse gains energy during propagation ($\eta > 0$), then it will emerge with a sharp spike, as shown in Fig. 4(b). Beam shaping will also occur if the two pulses have similar temporal envelopes, as shown in Figs. 5 and 6. In Fig. 5 we chose the two beams to be identical, transform-limited Gaussians. In Fig. 6 we chose a transform-limited weak beam and a strong beam that is linearly chirped and with a somewhat wider spectral width. Note the strong ringing caused by the temporal overlap of the two pulses.

7. CONCLUSION

In summary, we have derived an analytical expression for the two-beam-coupling gain of a photorefractive crystal when it is illuminated by two light beams that contain infinite trains of amplitude-stabilized pulses. We demonstrated that the photorefractive space-charge field reaches a quasi-steady-state value proportional to the local fringe visibility in the crystal. We find that the time-average intensity gain of each beam is proportional to the magnitude squared of the electric-field correlation of the interfering beams at the entrance face of the crystal. Consequently, the correlation between two optical pulse trains can be measured by performing two-beam coupling experiments in a photorefractive crystal. We have also shown that optical pulses will be shaped by their coupling in a photorefractive crystal, and we have derived analytic expressions describing how each pulse transforms during propagation through the crystal.

APPENDIX A: PULSE-SHAPE CALCULATIONS

We can use Eqs. (40a) and (40b) to calculate how the intensities of two interacting pulses will change with time because of beam coupling. In general, we must first choose the shapes of the incident pulses before the crystal and then calculate the normalized electric-field correlation function. In the example shown in Fig. 4, we chose one pulse to be transform limited and Gaussian in time and the other pulse also to be Gaussian in time, with the same spectral width, but chirped. We might generate such pulses by splitting a transform-limited Gaussian pulse into two pulses and sending one of the pulses through a Treacy grating pair.[28] This pulse will be chirped and temporally stretched. If the duration τ_{p1} of the stretched pulse (1) is q times the duration τ_{p2} of the unstretched pulse $\tau_{p1} = q\tau_{p2}$, then the normalized complex temporal amplitudes of these pulses can be expressed as

$$\mathcal{T}_1(t) = \exp\left[\frac{-2\ln 2(1 + i\sqrt{q^2 - 1})t^2}{\tau_{p1}^2}\right], \quad (42a)$$

$$\mathcal{T}_2(t - \tau_d) = \exp\left[-2\frac{(t - \tau_d)^2}{\tau_{p2}^2}\ln 2 + i\omega_0\tau_d\right], \quad (42b)$$

where τ_{p1} is the FWHM intensity width of the long pulse and ϕ_0 is a constant phase. Both pulses are Gaussian with the same spectral width $\Delta\omega = (4/\tau_{p2})\ln 2$, as can be shown by taking their Fourier transforms. Because the original pulse is assumed to be transform limited, the coherence function $\gamma^{(2)}$ is unity. The corresponding correlation function, calculated using Eq. (28), becomes

$$\Gamma(\tau_d) = \frac{\sqrt{2}\exp\left[-\frac{i}{2}\tan^{-1}\left(\frac{\sqrt{q^2 - 1}}{q^2 + 1}\right) - i\omega_0\tau_d\right]}{(q^2 + 3)^{1/4}} \times \exp\left[-\frac{2\ln 2}{q^2 + 3}(2 + i\sqrt{q^2 - 1})\frac{\tau_d^2}{\tau_{p2}^2}\right]. \quad (43)$$

If the average intensity of beam 1 is much smaller than that of beam 2, e.g., $\langle|E_1|^2\rangle \ll \langle|E_2|^2\rangle$, then substitution into Eq. (40a) yields

$$E_1(z,t) = E_{10}\{\mathcal{T}_1[t - (z/v)] + \sqrt{q}\Gamma(\tau_d)(e^{\eta z} - 1)\mathcal{T}_2[t - (z/v) - \tau_d]\}. \quad (44)$$

Substituting Eqs. (42) and (43) into Eq. (44), we can calculate the intensity of pulse 1 as a function of time and distance in the crystal. The results are shown in Figs. 4 and 5. [In Fig. 5 both beams are transform limited, so that $q = 1$ in Eqs. (41)–(44).]

In Fig. 6 we consider pulses with the same temporal width but different spectral widths and with a linear chirp on the spectrally wider beam. If the spectral width of pulse 2 is m times that of pulse 1, then the two pulses can be expressed as

$$\mathcal{T}_1(t) = \exp\left(-2\ln 2\frac{t^2}{\tau_p^2}\right), \quad (45)$$

$$\mathcal{T}_2(t - \tau_d) = \exp\left[-2\ln 2 \times (1 + i\sqrt{m^2 - 1})\frac{(t - \tau_d)^2}{\tau_p^2} + i\omega_0\tau_d\right]. \quad (46)$$

Pulse 1 is transform limited, and the coherence function $\gamma^{(2)}$ is unity. The corresponding correlation function, calculated using Eq. (28), is

$$\Gamma(\tau_d) = \frac{\sqrt{2}\exp\left[\frac{i}{2}\tan^{-1}\left(\frac{\sqrt{m^2 - 1}}{2}\right) - i\omega_0\tau_d\right]}{(m^2 + 3)^{1/4}} \times \exp\left[-\frac{2\ln 2}{m^2 + 3}(1 + m^2 + i\sqrt{m^2 - 1})\frac{\tau_d^2}{\tau_p^2}\right]. \quad (47)$$

Substituting Eqs. (45)–(47) into Eq. (44) and setting $q = 1$ (the two pulses are given the same temporal width), we obtain Fig. 6.

ACKNOWLEDGMENTS

We thank R. Pierce, J.-M. C. Jonathan, D. Mahgerefteh, and C. M. Caves for fruitful discussions. This research is supported by the Joint Services Electronics Program and contract F49620-88-C-9905 of the U.S. Air Force Office of Scientific Research. V. Dominic gratefully acknowledges fellowship support from the National Science Foundation and the Joint Services Electronics Program.

REFERENCES AND NOTES

1. L. Solymar, "Theory of volume holographic formation in photorefractive crystals," in *Electro-Optic and Photorefractive Materials*, P. Günter, ed. (Springer-Verlag, Berlin, 1987), pp. 229–245.
2. A. L. Smirl, G. C. Valley, K. M. Bohnert, and T. F. Boggess, Jr., "Picosecond photorefractive and free-carrier transient energy transfer in GaAs at 1 μm," IEEE J. Quantum Electron. **24**, 289–302 (1988).
3. A. L. Smirl, K. Bohnert, G. C. Valley, R. A. Mullen, and T. F. Boggess, "Formation, decay, and erasure of photorefractive gratings written in barium titanate by picosecond pulses," J. Opt. Soc. Am. B **6**, 606–615 (1989).
4. A. L. Smirl, G. C. Valley, R. A. Mullen, K. Bohnert, C. D. Mire, and T. F. Boggess, "Picosecond photorefractive effect in $BaTiO_3$," Opt. Lett. **12**, 501–503 (1987).
5. A. M. Johnson, A. M. Glass, W. M. Simpson, R. B. Bylsma, and D. H. Olson, "Microwatt picosecond pulse autocorrelator using photorefractive GaAs:Cr," in *OSA Annual Meeting*, Vol. 11 of 1988 Optical Society of America Technical Digest Series (Optical Society of America, Washington, D.C., 1988), p. 128.
6. A. M. Johnson, A. M. Glass, W. M. Simpson, and D. H. Olson, "Infrared picosecond pulse diagnostics using photorefractive beam coupling," in *Conference on Lasers and Electro-Optics*, Vol. II of 1989 Optical Society of America Technical Digest Series (Optical Society of America, Washington, D.C., 1989), p. 226.
7. A. M. Johnson, W. M. Simpson, A. M. Glass, M. B. Klein, D. Rytz, and R. Trebino, "Infrared picosecond pulse correlation measurements using photorefractive beam coupling and harmonic generation in $KNbO_3$ and $BaTiO_3$," in *OSA Annual Meeting*, Vol. 18 of 1989 Optical Society of America Technical Digest Series (Optical Society of America, Washington, D.C., 1989), p. 53.
8. V. Dominic, X. S. Yao, R. M. Pierce, and J. Feinberg, "Measuring the coherence length of mode-locked laser pulses in real time," Appl. Phys. Lett. **56**, 521–523 (1990).
9. F. P. Strohkendl, J. M. C. Jonathan, and R. W. Hellwarth, "Hole–electron competition in photorefractive gratings," Opt. Lett. **11**, 312–314 (1986).
10. Here we use the fact that the ensemble average of the derivative of a function equals the derivative of the ensemble average of the function. See, for example, A. Papoulis, *Probability, Random Variables, and Stochastic Process* (McGraw-Hill, New York, 1965), Chap. 9, pp. 314–318.
11. J. Feinberg, "Optical phase conjugation in photorefractive materials," in *Optical Phase Conjugation*, R. Fisher, ed. (Academic, New York, 1983), pp. 417–443.
12. R. Trebino, E. K. Gustafson, and A. E. Siegman, "Fourth-order partial-coherence effects in the formation of integrated-intensity gratings with pulsed light sources," J. Opt. Soc. Am. B **3**, 1295–1304 (1986).
13. J. W. Goodman, *Statistical Optics* (Wiley, New York, 1985), Chap. 3, pp. 63–68.
14. For example, if both of the optical fields are derived from the same mode-locked laser, then Eq. (6) will hold as long as the laser exhibits no long-term changes in the statistics of its phase fluctuations during an experiment. However, if the alignment of the mirrors of the laser should drift with time, for example, then the laser's pulse statistics might change, and Eq. (6) would no longer follow from Eq. (5).
15. The coupling coefficients η_{12} and η_{21} in the coupled-wave equations (21a) and (21b) will be slightly different if the term $\nabla(\nabla \cdot \mathcal{E})$ is retained. Namely, $\cos\theta$ will be replaced by $\cos\theta - \mathrm{Re}[(\hat{z}\cdot\hat{e}_i)(\hat{s}_i\cdot\hat{e}_i^*)]$ with $i = 1$ in Eq. (21a) and $i = 2$ in Eq. (21b), where $\hat{s}_1$ and $\hat{s}_2$ are the unit vectors along $\mathbf{k}_1$ and $\mathbf{k}_2$, respectively, $\hat{z}$ is a unit vector in the z direction, and we assume that the optical field amplitudes vary only along the z direction.
16. A. V. Alekseev-Popov, A. V. Knyaz'kov, and A. S. Saikin, "Recording volume amplitude-phase holograms in a lead-lanthanum zirconate-titanate ceramic," Sov. Tech. Phys. Lett. **9**, 475–477 (1983).
17. K. Walsh, T. J. Hall, and R. E. Burge, "Influence of polarization state and absorption gratings on photorefractive two-wave mixing in GaAs," Opt. Lett. **12**, 1026–1028 (1987).
18. Y. Lee, "Studies of the photorefractive effect in barium titanate: higher-order spatial harmonics and two-beam energy coupling," (University of Southern California, Los Angeles, Calif., 1989).
19. R. M. Pierce, R. S. Cudney, G. D. Bacher, and J. Feinberg, "Measuring photorefractive trap density without the electro-optic effect," Opt. Lett. **15**, 414–416 (1990).
20. H. J. Eichler, U. Klein, and D. Langhans, "Coherence time measurement of picosecond pulses by light-induced grating method," Appl. Phys. **21**, 215–219 (1980).
21. Z. Vardeny and J. Tauc, "Picosecond coherence coupling in the pump and probe technique," Opt. Commun. **39**, 396–400 (1981).
22. R. Baltrameyunas, Yu. Vaitkus, R. Danelyus, M. Pyatrauskas, and A. Piskarskas, "Applications of dynamic holography in determination of coherence times of single picosecond light pulses," Sov. J. Quantum Electron. **12**, 1252–1254 (1982).
23. S. L. Palfrey and T. F. Heinz, "Coherent interactions in pump–probe absorption measurements: the effect of phase gratings," J. Opt. Soc. Am. B **2**, 674–678 (1985).
24. W. L. Nighan, Jr., T. Gong, L. Liou, and P. M. Fauchet, "Self-diffraction: a new method for characterization of ultrashort laser pulses," Opt. Commun. **69**, 339–344 (1989).
25. In Ref. 8 we defined the coherence time of the pulse as one-half of the FWHM of the field correlation function. This definition leads to a coherence time = $\tau_c = (2\ln 2)/(\pi\Delta\nu)$ for an optical field having a Gaussian power spectral density with a FWHM of $\Delta\nu$ (Hz). With this definition the coherence time τ_c equals the pulse duration τ_p for a transform-limited pulse. A more common definition[12] of τ_c for cw beams is $\tau_c = \int_{-\infty}^{\infty}|\Gamma(\tau_d)|^2\,d\tau_d$. In this case $\tau_c = [(2\ln 2)/\pi]^{1/2}\,1/(\Delta\nu)$ for an optical field having a Gaussian spectrum with a FWHM of $\Delta\nu$ (Hz).
26. D. Krokel, N. J. Halas, G. Giuliani, and D. Grischkowsky, "Dark-pulse propagation in optical fibers," Phys. Rev. Lett. **60**, 29–32 (1988).
27. A. M. Weiner, J. P. Heritage, R. J. Hawkins, R. N. Thurston, E. M. Kirschner, D. E. Leaird, and W. J. Tomlinson, "Experimental observation of the fundamental dark soliton in optical fibers," Phys. Rev. Lett. **61**, 2445–2448 (1988).
28. E. D. Treacy, "Optical pulse compression with diffraction gratings," IEEE J. Quantum Electron. **QE-5**, 454–458 (1969).